공학박사 학위논문

AMINE-FUNCTIONALIZED HIGHLY POROUS
HYBRID MATERIALS FOR OPHTHALMIC
DELIVERY

안용 약물 전달을 위한 아민 기능화

초다공성 하이브리드 재료 연구

2019 년 2 월

서울대학교 대학원

협동과정 바이오엔지니어링 전공

김 세 나

AMINE-FUNCTIONALIZED HIGHLY POROUS

HYBRID MATERIALS FOR OPHTHALMIC

DELIVERY

안용 약물 전달을 위한 아민 기능화

초다공성 하이브리드 재료 연구

지도 교수 최 영 빈

이 논문을 공학박사 학위논문으로 제출함

2019 년 2 월

서울대학교 대학원

협동과정 바이오엔지니어링 전공

김 세 나

김세나의 공학박사 학위논문을 인준함

2019 년 2 월

위 원 장 _____최 진 욱_____ (인)

부위원장 _____최 영 빈_____ (인)

위   원 _____이 정 찬_____ (인)

위   원 _____정 기 훈_____ (인)

위   원 _____박 한 수_____ (인)

Ph. D. Dissertation

AMINE-FUNCTIONALIZED HIGHLY POROUS HYBRID MATERIALS FOR OPHTHALMIC DELIVERY

BY

SE NA KIM

FEBURARY 2019

INTERDISCIPLINARY PROGRAM IN BIOENGINEERING

THE GRADUATE SCHOOL

SEOUL NATIONAL UNIVERSITY

AMINE−FUNCTIONALIZED HIGHLY POROUS

HYBRID MATERIALS FOR OPHTHALMIC

DELIVERY

BY

SE NA KIM

INTERDISCIPLINARY PROGRAM IN BIOENGINEERING

THE GRADUATE SCHOOL

SEOUL NATIONAL UNIVERSITY

THIS DISSERTATION IS APPROVED FOR

THE DEGREE OF DOCTOR OF PHILOSOPHY

FEBURARY 2019

DOCTORAL COMMITTEE:

Chairman	*Jin Wook Choi, Ph. D.*
Vice Chairman	*Young Bin Choy, Ph. D.*
Member	*Jung Chan Lee, Ph. D.*
Member	*Kee Hoon Jung, Ph. D.*
Member	*Han Su Park, Ph. D.*

Abstract

AMINE–FUNCTIONALIZED HIGHLY POROUS HYBRID MATERIALS FOR OPHTHALMIC DELIVERY

By

Se Na Kim

Interdisciplinary Program in Bioengineering

The Graduate School

Seoul National University

This dissertation is focused on the design, synthesis, surface functionalization, analysis and evaluation of highly porous hybrid materials to enhance the therapeutic effect of ocular drug delivery systems. Ophthalmologic diseases have long been a challenging issue in the field of drug delivery. Numerous studies have been conducted with the goal of increasing the delivery efficiency of eye drop delivery, which accounts for 90% of ophthalmic drug delivery regimens. Topical delivery of ophthalmic drugs poses the problem

of low drug bioavailability (< 5%), as conventional eye drops are cleared rapidly from the surface of the eye due to blinking and rapid tear turnover, mostly drained via the nasolacrimal duct.

To enhance ocular drug bioavailability after topical administration to the eye, it is necessary for drug carriers to remain on the eye surface for a longer period. A variety of micro- and nano-particles have been proposed to resolve this issue, among which particles composed of mucoadhesive materials have received a great deal of interest. Mucoadhesive particles are known to adhere to the mucin present on the eye surface, and therefore, have the potential to improve the retention of drugs in the preocular space.

To develop topical eye drops using highly porous hybrid materials with mucoadhesive functionality, I propose a metal-organic framework (MOF), $NH_2-MIL-88(Fe)$, as a novel carrier for topical drug delivery to the eye. $NH_2-MIL-88(Fe)$ particles were prepared via a solvothermal synthesis method and their structure was confirmed by powder X-ray diffraction, Fourier transform infrared analysis, thermogravimetric analysis, electron microscopy, and N_2 adsorption-desorption measurements. When brimonidine, an anti-glaucoma medicine, was encapsulated into $NH_2-MIL(Fe)-88$ (i.e., $NH_2-MIL-88(Fe)/Br$), the drug was loaded at 121.3 mg/mg and released in a sustained manner for up to 12 h. The $NH_2-MIL-88(Fe)/Br$ exhibited mucoadhesive properties and remained on rabbit eyes for a period of up to 4 h. Consequently,

a high concentration of brimonidine was found in tears for a prolonged period after the administration of $NH_2-MIL-88(Fe)/Br$, which resulted in a greater than two-fold increase in drug bioavailability and the activity period compared with those of Alphagan-P, a brimonidine eye drop already approved for clinical use. Hence, $NH_2-MIL-88(Fe)$ appears to be a promising carrier for topical delivery to the eye that provides enhanced bioavailability for ocular drugs.

I also propose the use of amine-grafted SBA-15 particles (i.e., APS-SBA-15) for topical delivery of dexamethasone to the eye. Owing to the surface functionalization of amine groups, dexamethasone, an anionic drug, can be effectively loaded in the mesopores of APS-SBA-15 at loading quantities of 68.23 μg/mg to yield DXS@APS-SBA-15, which, in turn, can be released in a sustained manner for 12 h. DXS@APS-SBA-15 exhibited pronounced mucoadhesive properties because of the presence of both amine and hydroxyl groups in the particles. Therefore, when administered to rabbit eyes in vivo, the DXS@APS-SBA-15 appeared to adhere to the mucin and stay longer on the eye surface, where the drug could be released slowly. Hence, the DXS@APS-SBA-15 introduced herein resulted in > 1.8-fold improvement in the in vivo ocular bioavailability of dexamethasone compared to the conventional eye drop, Maxidex.

Through these studies, I concluded that amine functionalized metal-organic frameworks (MOFs) and amine grafted mesoporous

silica particles are promising carriers for enhanced bioavailability of topically-delivered ocular drugs. They are also expected to be widely used in various mucin-rich organs, not limited to ophthalmic drug delivery systems.

Contents

List of Tables

List of Figures

Chapter 1

Introduction

1.1　Ophthalmic Drug Delivery Systems

The anatomic and physiologic structure of the eye is very complex. The structure of the eye consists of anterior and posterior segments (Figure 1.1). Tissues such as the conjunctiva, cornea, iris, ciliary body, aqueous humor, and lens make up the anterior portion. The posterior segment of the eye includes the choroid, sclera, neural retina, retinal pigment, epithelium, optic nerve and vitreous humor. Diseases that affect the anterior segment include anterior uveitis, glaucoma, allergic conjunctivitis, and cataract, whereas diabetic retinopathy and age-related macular degeneration are the most prevalent

diseases in the posterior segment.

Worldwide, an estimated 180 million people are visually disabled. Of these, between 40 and 45 million individuals are blind. Approximately 50% of the world's blind suffer from cataract [1]. The majority of the remaining people are blind from conditions that include, among others, trachoma, glaucoma, onchocerciasis, and trachoma (Figure 1.2). Despite a half century of effort, the global burden of blindness is growing largely because of population growth and ageing. In order to lower the blindness rate of eye diseases, it is very important to receive prompt and accurate diagnosis as well as appropriate treatment continuously at the correct time. For this purpose, various drug delivery systems for treating eye diseases have been developed.

In this chapter, I provide an overview of various conventional and novel ophthalmic drug delivery systems developed to deliver ocular drugs to diseased tissues for the treatment of eye diseases.
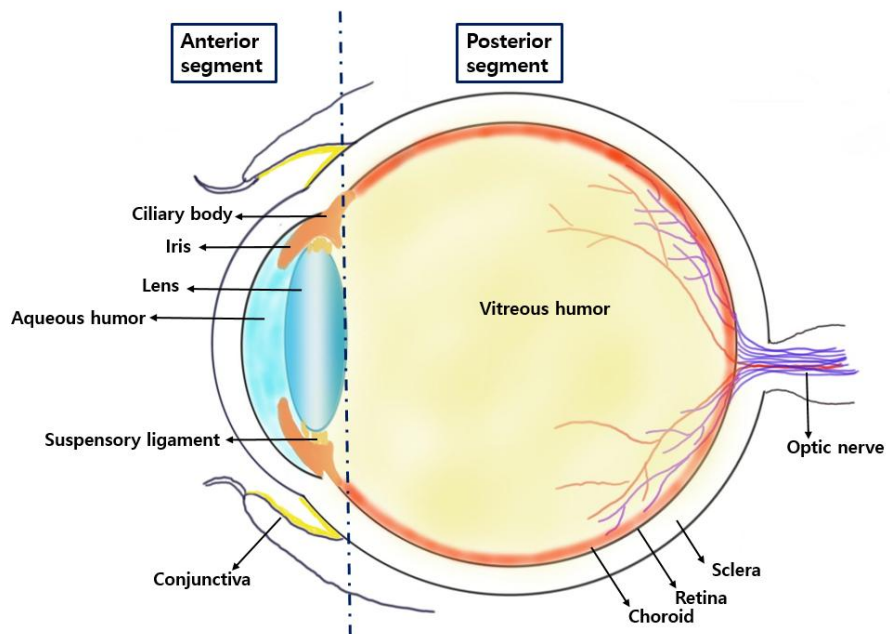
Figure 1.1. Schematic representation of the structure of the human eye.
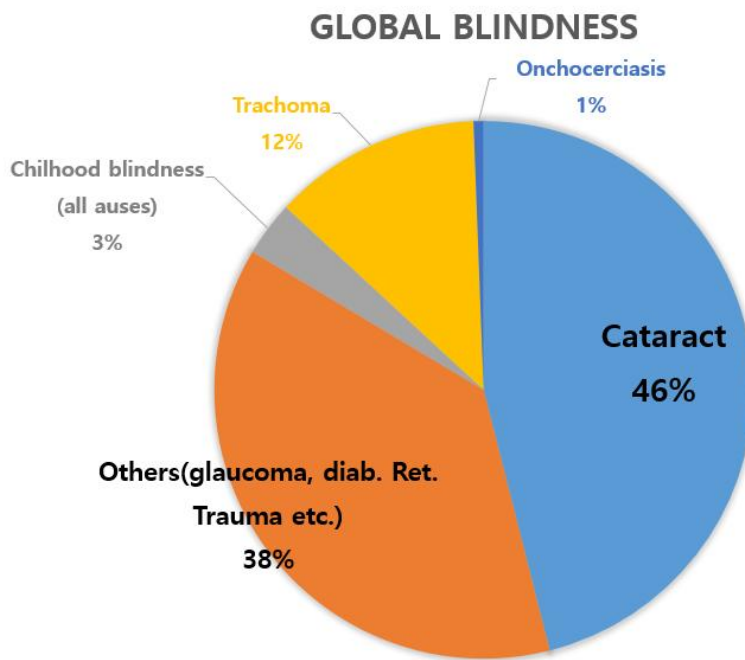
Figure 1.2. Schematic representation of cause of global blindness [1].

1.1.1 Conventional Ocular Drug Delivery Systems

Topical instillation of eye drops into the lower precorneal pocket is the most widely preferred non−invasive route of drug administration to treat ocular diseases. Eye drops account for 90% of marketed ophthalmic formulations because of patient compliance. However, most of the topically administered drug is lost due to eye blinking and only 20% of the instilled dose is retained in the precorneal pocket. The amount of drug absorbed is only 5% of the amount administered.

The concentration of a drug acts as a driving force for passive diffusion across cornea tissue. Therefore, for efficient ocular drug delivery using eye drops, longer drug cornea contact time with high corneal permeation is required. Depending on the location of the target ocular tissue, a variety of drug delivery methods are available (Figure 1.3). Several studies have been conducted to improve the residence time of drugs and corneal penetration. The developed conventional formulations are briefly summarized below.
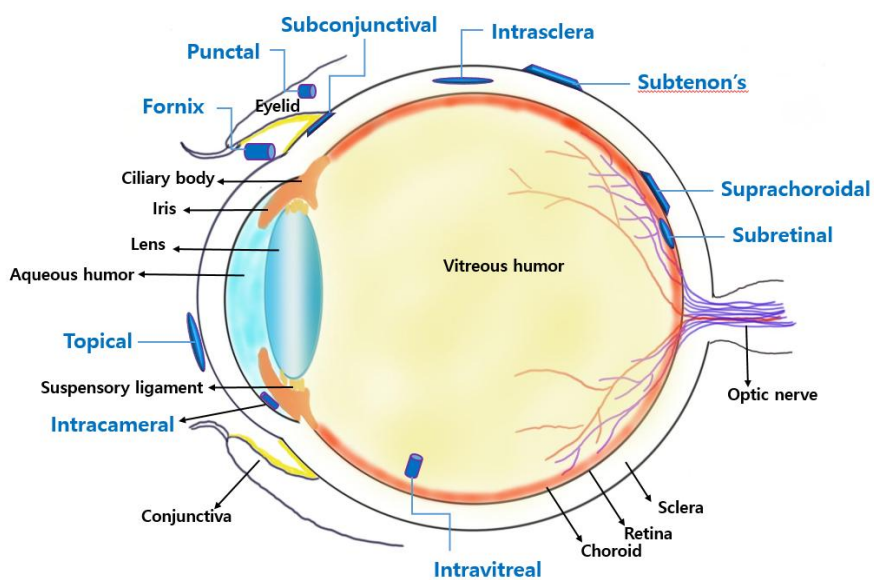
Figure 1.3. Development of formulations and delivery systems for ocular drug delivery [2].

- Topical liquid/solution eye drops

Topical drops are the most convenient, immediately active, patient compliant, safe, and non-invasive route of ocular drug administration. After topical drop instillation, an eye drop solution provides pulse drug permeation, followed by rapid decline of the drug concentration. The kinetics of drug concentration decline follows a first order. Therefore, to enhance drug contact time and permeation, various additives may be added to eye drop solutions such as viscosity and/or permeation enhancers.

- Emulsions

An emulsion-based formulation offers an advantage to improve both the bioavailability and solubility of drugs. There are two types of emulsions: water in oil (w/o) and oil in water (o/w) emulsion systems. For ophthalmic drug delivery, o/w emulsion is widely used because they it results in less irritation and better ocular tolerance.

- Suspensions

Suspensions are a class of immediately active and non-invasive ocular topical drop drug carrier systems. Suspensions may

contain finely divided insoluble API in an aqueous solvent. Suspension particles remain in precorneal pockets and thereby improve drug contact time as well as the duration of action relative to the drug solution. The particle size is expected to result in optimum drug activity. Several suspension formulations are marketed worldwide to treat ocular bacterial infections.

- Ointments

Ophthalmic ointments contain a mixture of a semisolid and a solid hydrocarbon with a melting point at the physiological ocular temperature (34 ℃). The choice of hydrocarbon is dependent on biocompatibility. Ointments help to improve ocular bioavailability and sustain drug release.

1.1.2 Novel Ocular Drug Delivery Systems

In addition to conventional methods, various advanced technologies have been introduced to improve the therapeutic effect of ophthalmic drug delivery and are briefly summarized below. For the treatment of eye diseases, many approaches have been developed using nanotechnology. Currently, nanotechnology-based ocular drug delivery formulations comprise one of the novel approaches being pursued for both posterior and anterior segment drug delivery. An appropriate particle size using nanotechnology can be designed to ensure adequate bioavailability, low irritation, and ocular tissue compatibility.

Several nanocarriers, such as nanosuspensions, nanoparticles, nanomicelles, and liposomes have been developed for novel ocular drug delivery systems (Table 1.1). A variety of devices such as drug loaded contact lens, microneedles, and implants have also been developed. Some of devices have shown promising results for improving drug bioavailability to the eye. The systems that have been developed and reported in the literature to date are briefly summarized below.

Table 1.1. Summary of recent developments with nanoparticles as ocular drug delivery vehicles [2]

Drug	Polymer	Features
Carboplatin	Chitosan Sodium alginate	−Carboplatin loaded NPs demonstrated elevated and sustained anti−proliferative activity in a retinoblastoma cell line (Y−79), with IC50 of 0.56 and 0.004 μg/mL for free carboplatin and carboplatin loaded NPs, respectively.
5−FU	Chitosan Sodium alginate	−CH coated SA−CH nanoparticles (CH−SA−CH NPs) loaded with 5−FU showed significantly higher concentration of 5−FU in aqueous humor as compared to SA−CH 5−FU loaded NPs and 5−FU solution. The higher C_{max} was achieved in case of CH−SA−CH NPs (24.67 μg/mL) compared to 5−FU solution (6.14 μg/mL).
Sparfloxacin	PLGA	−After topical application, sparfloxacin−loaded nanoparticles were retained for a longer duration on the corneal surface as compared to an aqueous solution, which was drained rapidly from the corneal surface. Also, in vitro release studies revealed an extended release of sparfloxacin.
Brimonidine tartrate	Sodium alginate Eudragit RS 100 Eudragit RL 100	−Brimonidine tartrate−loaded nanoparticles provided prolong drug release over a period of 8 h after topical instillation to albino rabbits. −The AUC (⊿IOP vs time) for the selected nanoparticles formulations were about seven times higher than that of eye drop formulations in rabbit eye.
Levofloxacin	PLGA	−The nanosuspensions was retained for the longer time on rabbit eye surface and drained out slowly compared to marketed formulation. −Results of ex−vivo transcorneal permeation study across excised goat cornea revealed that levofloxacin from the marketed formulation was permeated 36.9% in 4 h whereas levofloxacin from PLGA nanoparticles was permeated 47.43% in 4 h across cornea.
Diclofenac sodium	PLGA	−An extended DS release was observed from the nanoparticles under in vitro conditions. −The developed polymer nanoparticles formulation was non−irritant to cornea, iris, and conjunctiva for as long as 24 h after application.
Pilocarpine	PLGA	−The in vivo miosis studies showed that the duration of miotic response increased by 40% for the nanoparticles compared to the eye drops.
Gatifloxacin Prednisolone	Eudragit−RS100/RL100, coating with hyaluronic acid	−In vitro release studies revealed prolonged drug release compared to the free drugs with no burst effect Nanoparticles formulation showed better bioavailability of gatifloxacin in rabbit eye with 1.76 fold increase in Cmax of gatifloxacin in the aqueous humor in comparison to the eye drops.
Cloricromene	Eudragit	−Nanosuspension enhanced stability of the ester drug for several months as compared to an Cloricromene aqueous solution.

- Nanosuspensions

Nanosuspensions are colloidal dispersion formulations of submicron drug particles stabilized by surfactants. They have been demonstrated to be a promising approach for the delivery of hydrophobic drugs. They have several advantages such as ease of eye drop preparation, sterilization, increased precorneal residence time, less irritation, and enhancement of the ocular bioavailability of hydrophobic drugs.

- Nanoparticles

Nanoparticles are carriers with a size range of 10 to 500 nm. For ophthalmic drug delivery, nanoparticles are mostly composed of proteins, lipids, natural or synthetic polymers such as poly(lactide-co-glycolide) (PLGA), chitosan, albumin, polycaprolactone, sodium alginate, and polylactic acid (PLA).

- Nanomicelles

Nanomicelles are the most frequently used systems to formulate therapeutic drugs in clear solutions. In general, nanomicelles are prepared using amphiphilic molecules. Because the method is non-invasive, topical drug formulations using nanomicelles have attracted significant interest in the market. For both the anterior and posterior eye segments, nanomicelles can be applied by selecting appropriate surfactants/polymers.

- Liposome

Liposomes are lipid vesicles with several phospholipid bilayers surrounding an aqueous core. The size of liposomes generally ranges from 0.08 to 10.00 μm and liposomes can be classified as small unilamellar vesicles (size range; 10–100 nm), large unilamellar vesicles (size range; 100–300 nm) and multilamellar vesicles.

- Contact lens

Contact lenses are curved plastic disks designed to cover the cornea. After application, drug loaded contact lens adhere to the film of tears over the cornea due to surface tension. Drug loaded contact lens have been developed for ocular delivery of numerous drugs such as antihistamines, antimicrobials, and β-blockers.

- Implants

Usually for drug delivery to posterior ocular tissues, implants are specifically designed to provide localized drug release over an extended period. These implantable devices help avoid multiple intraocular injections and the associated complications. Ocular implants are available as non-biodegradable and biodegradable drug releasing devices.

- Microneedles

Microneedle-based techniques are minimally invasive methods of drug delivery to posterior ocular tissues. Microneedles are designed to penetrate only hundreds of microns into sclera, so that damage to ocular tissues may be avoided.

1.1.3 Current Drawbacks

Drug delivery to targeted ocular tissues has been a major challenge to ocular scientists for several decades. Tremendous efforts are being made toward the development of non-invasive and patient compliant techniques using novel drug delivery strategies. However, topical instillation is still the most widely preferred safe route of drug administration to treat diseases in the anterior segment. In the clinical area, conventional methods such as eye drops account for 90% of the marketed ophthalmic formulations. Nonetheless, the ocular bioavailability is very low with topical drop administration.

Numerous physiological and anatomical constraints such as nasolachrymal drainage, tear turnover, reflex blinking, and ocular static and dynamic barriers pose a challenge. For this reason, it is difficult for the drug to be absorbed deep into the eyeball tissue. Hence, less than 5% of the topically applied dose reaches the target ocular tissues. A variety of drug delivery formulations have been developed using mucoadhesive materials to enhance the drug residence time in the pre-ocular space. However, they have limitations for clinical applications because they require complex manufacturing processes.

There is a need to develop and evaluate new topical drug delivery carriers to the eye. These new carriers should not only be biocompatible, but also have sufficient mucoadhesion

properties, and should be produced with relatively simple processes.

1.2 Mucoadhesive Drug Delivery Systems

Mucoadhesion is commonly described as the adhesion between materials and mucosal surfaces [3]. Over the past few decades, mucoadhesive drug delivery systems have received a great deal of attention. Mucoadhesive formulations may be designed to enable prolonged retention time at the site of application, providing a controlled drug release rate for improved therapeutic outcomes. The mucoadhesive ability of a formulation is reliant on a variety of factors, such as the physicochemical properties of the prepared formulation and the nature of the mucosal tissue. Various mucoadhesive drug delivery systems (buccal, nasal, ocular, gastro, vaginal, and rectal) have been developed and evaluated for various aspects of mucoadhesion, mucoadhesive materials, factors affecting mucoadhesion, and evaluation methods in drug delivery applications.

In the last two decades, mucoadhesion has shown great potential for prolonging the residence time of mucoadhesive formulations through specific mucosal routes in drug delivery applications. Mucoadhesive-based local and topical delivery systems have demonstrated enhanced bioavailability. The mucoadhesive properties of these particles can largely be

explained by the formation of ionic complexes and hydrogen bonds between the mucoadhesive material and mucin, which can be found in materials possessing positively charged amine groups, as well as hydroxyl and carboxyl groups.

In this chapter, to provide a detailed understanding of mucoadhesion, I review the structure and function of mucous membranes, theories of mucoadhesion, bioadhesive polymer materials and techniques.

Mucous membranes have moist surfaces covering the walls of the organs of respiratory and gastrointestinal organs, such as the genital organs, the inner parts of the eyes, nasal and oral cavities [4-7]. Table 1.2 shows anatomical differences in the mucus membrane. To explain mucoadhesion, various theoretical models exist for at least some of the experimental observations. Unfortunately, each model can only explain a limited number of the diverse range of interactions that constitute the bioadhesive bond. There are four main theories.

- Adsorption Theory of Mucoadhesion
- Electrostatic Theory of Mucoadhesion
- Wetting Theory of Mucoadhesion
- Diffusion Theory of Mucoadhesion

Table 1.2. Anatomical differences of the mucus membrane [3]

Mucus membrane	Relevant anatomical features
Buccal	Buccal mucosa surface area approximately 30 cm^2/ Comprised of three distinct layers – epithelium, basement membrane, and connective tissues/ Buccal mucosa, sublingual are soft palate nonkeratinized tissue, and gingival are hard palate keratinized tissue/ Thickness of buccal epithelium is in the range of 500–800 µm, 40–50 cells thick/ Mucus secreted by salivary glands, as a component of saliva, forming a 0.1–0.7 mm thick layer/ Turnover time for buccal epithelium 5–6 days/ Permeability barrier property of oral mucosa due to intercellular materials derived from membrane-coating granules
Nasal	Nasal cavity surface area 160 cm^2/Lined with mucous membrane containing columnar cells, goblet cells, and basal cells/ Columnar cells are covered with cilia, apart from the anterior part of the nasal cavity/ Both keratinized and nonkeratinized epithelial cells present depending upon location within nasal cavity/ Cilia responsible for mucociliary clearance/ Mucus secreted by the submucosal glands and the goblet cells, forming a mucus layer approximately 5–20 µm thick/ Nasal cavity length approximately 60 mm/ Nasal cavity volume approximately 20 mL/ Turn-over time for mucus is usually 10–15 min
Ocular	Cornea is composed of five layers – epithelium, Bowman's layer, stroma, Descemet's membrane, and endothelium/ Epithelium consists of 5–6 layers of cells, with the cells of the basal layer being columnar, and the outermost cells flattened polygonal cells/ Tight junctions present between the basal cells of the corneal epithelium/ At the corneal margin, the conjunctiva is structurally continuous with the corneal epithelium/ The conjunctival tissue is permeable to molecules up to 20,000 Da, whereas the cornea is impermeable to molecules greater than 5000 Da/ The conjunctiva contains around 1.5 million goblet cells, which synthesize secretory mucins and peptides/ A volume of about 2–3 µL of mucus of secreted daily/ A turnover of the mucus layer occurs in approximately 15–20 h/ Exposed part of the eye is covered by a thin fluid layer – percorneal tear film
Vaginal	Length of vagina varies from 6 to 10 cm/The epithelial layer consists of the lamina propia and stratified squamous epithelium/ A cell turnover of about 10–15 layers is estimated to be in the order of 7 days/ Although there are no glands in the vagina mucosa, the surface is usually covered with vaginal fluid/ Major components of vaginal fluid are cervical mucus and vaginal fluid from the well-vascularized mucosa/ The volume, viscosity, and pH of the cervical mucus vary with age and during the menstrual cycle
Rectal	Length approximately 15–20 cm/Surface area of approximately 300 cm^2/ Epithelium consists of a single layer of cylindrical cells and goblet cells secreting mucus/ Flat surface, without villi, and with three major fold, the rectal valves/ Approximately 3 mL of mucus with a neutral pH spread over the surface

Mucoadhesive polymers have abundant hydrophilic groups, such as amine, amide, carboxyl, hydroxyl, carboxyl, and sulfate (Table 1.3). These groups attach to the cell membrane or mucus moieties through various interactions (e.g., hydrophobic interactions, electrostatic interactions, or hydrogen bonding). Table 1.4 shows the factors affecting mucoadhesion. For bioadhesive drug delivery systems, an ideal polymer should have the following characteristics;

- nonabsorbable
- nontoxic
- nonirritable
- form a strong noncovalent bond with the mucus layer
- adhere quickly to moist tissue

Table 1.5 shows the chemical structures of several bioadhesive polymers commonly used in modern drug delivery.
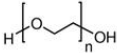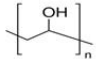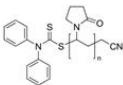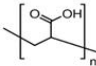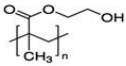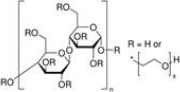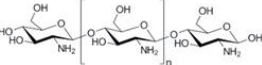
Table 1.3. Viscosifying polymers screened for ocular mucoadhesive capacity [2]

Polymer	Charge	Mucoadhesive capacity
Poly(acrylic acid) (neutralized)	Anionic	+++
Carbomer (neutralized)	Anionic	+++
Hyaluronan	Anionic	+++
Chitosan	Cationic	++
Poly(galacturonic acid)	Anionic	++
Na alginate	Anionic	++
Pectin	Anionic	++
Poloxamer	Non-ionic	+
Hydroxypropylmethylcellulose	Non-ionic	+
Methylcellulose	Non-ionic	+

Mucoadhesive capacity: +++: excellent; ++: good; +: absent.

Table 1.4. Factors Affecting Mucoadhesion

Factor		Characteristics, examples	Ref.
Properties of the mucoadhesive polymer	Molecular weight	Low-molecular-weight polymers penetrate the mucus layer better. / High molecular weight promotes physical entangling. / The optimum molecular weight is between 10^4 and 4×10^6 Dal.	[2, 7, 8]
	Polymer chain flexibility	Required for diffusion of chains and their entanglement with mucin. / For polymers with high levels of linkage, the mobilities of the individual polymer chains decrease, leading to decreases in mucoadhesion strength.	17,21 [7, 9]
	Ability to form hydrogen bonds	Presence of functional groups able to form hydrogen bonds (COOH, OH, etc.).	[9]
	Concentration	Affects the availability for penetration of long polymer chains into the mucus layer; important mainly for liquid and viscous DDS.	[6]
	Extent of swelling of polymer or DDS	Swelling of the polymer allows mechanical entangling because of the exposure of polymer chains and subsequent formation of hydrogen bonds and/or electrostatic interactions between the polymer and components of the mucosa.	[7]
Environmental factors	pH	Changes in pH lead to differences in the extent of dissociation of functional groups in carbohydrate sequences or polypeptide amino acid sequences, as well as in the polymer.	[9, 10]
	Pressure	Affects the depth of diffusion of chains. / Cannot be controlled for systems used in the GIT.	[4, 11]
	Duration of initial contact	Determines the extent of swelling and diffusion of polymer chains. Cannot be controlled for systems used in the GIT.	[4, 11]
	Moistening	Moistening is required to allow the mucoadhesive polymer to spread over the surface and create a "macromolecular network" of sufficient size for the interpenetration of polymer and mucin molecules and to increase the mobility of polymer chains. / However, there is a critical level of hydration for mucoadhesive polymers characterized by optimum swelling and bioadhesion.	[4, 12]
	Presence of metal ions	Interaction with charged groups of polymers and/or mucus can decrease the number of interaction sites and the tightness of mucoadhesive bonding.	[4]
Physiological factors	Rate of renewal of mucosal cells	Varies extensively for different types of mucosa. Limits the persistence of bioadhesive systems on mucosal surfaces.	[12]
	Tissue movement	On consumption of liquid and food, speaking, peristalsis in the GIT.	[4, 8]

Table 1.5. Chemical structures of some bioadhesive polymer used in drug delivery [3]

Polymer	Chemical structures
Poly (ethylene glycol)	
Poly (vinyl alcohol)	
Poly (vinyl pyrrolidone)	
Poly (acrylic acid)	
Poly(hydroxyethyl methacrylate)	
Hydroxyethyl cellulose	
Chitosan	

1.3 Highly Porous Materials for Drug Delivery Systems

In the field of health, one significant challenge is the efficient delivery of therapeutic drugs to the patient using non-toxic carriers. However, most of the current carriers show poor drug loading (less than 5 wt%) and/or rapid release of drugs, which are simply anchored or adsorbed at the external surface of the carrier material [13]. In this context, highly porous materials with the ability to adjust their structures and porosities for high loadings and better drug interactions are ideal as carriers for drug delivery applications. A variety of porous materials have been reported in academia. Among them, I focus on the two major materials that have recently received great attention in the field of drug delivery.

1.3.1 Metal-Organic Frameworks

MOFs are crystalline organic-inorganic hybrid structures comprised of metal ions or clusters and multidentate organic linkers connected to metal nodes in one-, two-, or three-dimensional networks (Figure 1.4) [14, 15]. Owing to their unique textural properties (large surface areas, uniform pore sizes and large pore volumes) and diverse functionalization through post-synthetic chemical treatments [16, 17], MOFs have attracted a great deal of interest in recent years for potential applications in adsorption/separation, gas storage, catalysis, and drug delivery systems (Figure 1.5) [16, 18, 19].

For drug delivery applications using MOFs, diverse methods were developed in the last twenty years. Because MOFs can exhibit remarkably high surface areas with large pore sizes, they have also been considered for applications in loading and controlled/sustained release of several therapeutic molecules [20]. Horcajada et al [13]. loaded anticancer and antiviral agents into MOFs. Morris et al [21]. encapsulated and delivered nitric oxide gas and a vasodilator agent. Lin et al [22]. reported the use of MOFs for the co-delivery of siRNA and the anticancer cisplatin molecule to enhance the therapeutic effect.

24

Table 1.6 shows a list of some of the types of MOFs and their biomedical applications. Some of the major advantages of MOFs compared with other organic (e.g., micelles, biopolymers and liposomes) and inorganic (e.g., zeolites, metallic nanoparticles) drug delivery systems are their high drug loading capacities and the possibility of chemically functionalizing the surface of the materials to enhance drug affinity.
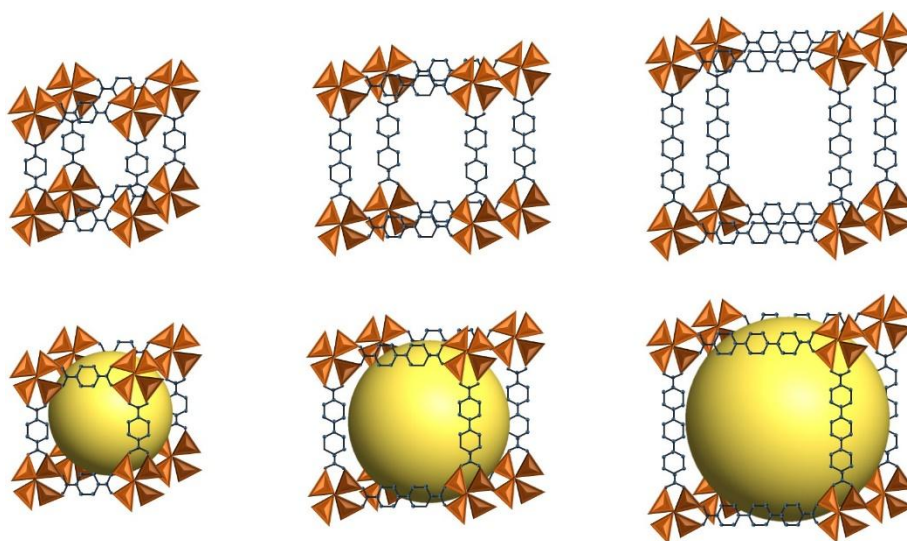
Figure 1.4. Schematics of metal organic frameworks [23].
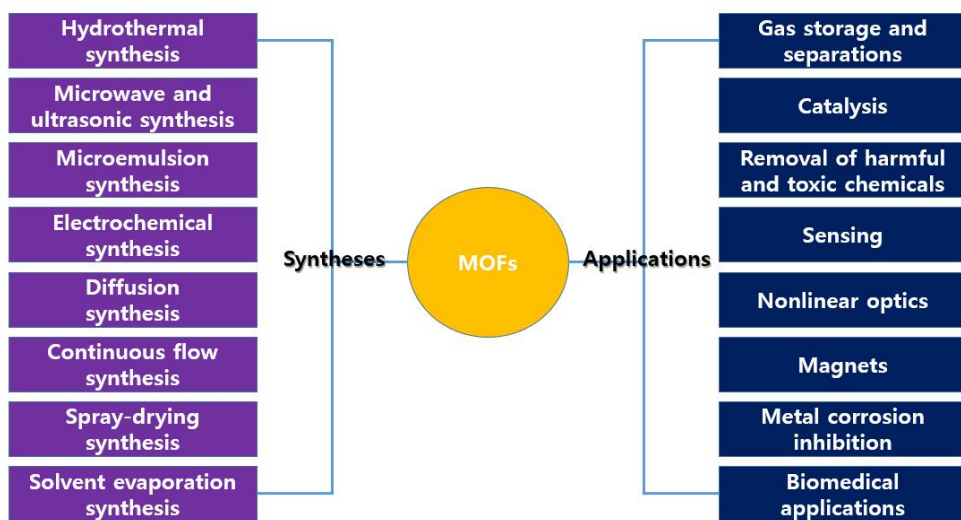
Figure 1.5. Schematics showing the synthesis and applications of MOFs [24].

Table 1.6. List of some of the types of MOFs and their biomedical applications.

MOFs	Biomedical Applications	Ref
ZIF-8	Cancer (doxorubicin)	[25]
UIO-66	Cancer (siRNA and cisplatin)	[26]
IRMOF-3	Cancer (paclitaxel)	[27]
Hf-TCPP	Cancer (radiation therapy)	[28]
UIO-66	Cancer (photodynamic therapy)	[29]
MIL-100	Cancer(photo theranostics)	[30]
Cu-BTT	Gastroenterology (gastro transmitter)	[31]
Mn-BTC	MRI	[32]
Gd-MOF	MRI	[33]

1.3.2 Mesoporous silicas

Since the first article using MCM□41 (Mobil Composition of Matter No. 41) mesoporous silica particles (MSPs) as a drug delivery system in 2001[34], the last several years have seen an exponential increase in research on biomedical application of MSPs (Figure 1.6). MSPs with unique mesoporous structures (Table 1.7) and large surface areas have been explored as effective drug delivery carriers for a variety of therapeutic agents to treat various kinds of diseases including cancer, diabetes, and inflammation [35−37]. Table 1.8 shows a list of some of the types of mesoporous materials and their biomedical applications.

Figure 1.6. The statistics of the paper indexed in the ISI web of science by the topic of "mesoporous silica" and "drug delivery "[39].
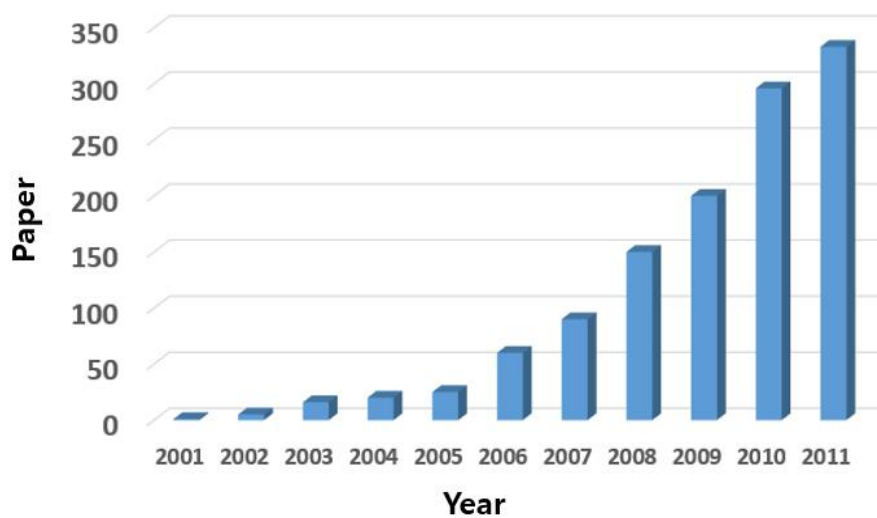
Table 1.7. Structural range of ordered mesoporous materials [38].

	Crystal class	Structural examples
Lamellar	-	MCM-50
2D cylindrical	Hexagonal	MCM-41
	Rectangular	SBA-8
3D cylindrical	Hexagonal	IBN-9
	Cubic	MCM-48, AMS-10
3D cage	Hexagonal	SBA-2
	Cubic	SBA-1, KIT-5, SBA-16, AMS-8
	Orthorhombic	FDU-13
	Tetragonal	FDU-11
		AMS-9

Table 1.8. List of some of the types of mesoporous silicas and their biomedical applications.

Materials	Biomedical Applications	Ref
SBA-15	Anti-inflammatory (ibuprofen)	[40]
SBA-15	Anti-inflammatory (naproxen)	[41]
MCM-41	Anti-inflammatory (naproxen)	[42]
FA-MSN	Cancer therapy (doxorubicin)	[43]
SBA-15	Estrogenic (alendronate)	[44]
MCM-41	Estrogenic (alendronate)	[44]
MCM-48	Estrogenic (alendronate)	[45]
SBA-15	Antibiotics (erythromycin)	[46]

1.4 Research Aim

Currently, for topical drug delivery to the eye, some materials are being used (e.g. micelles, liposomes, emulsions) but are, for the most part, still unsatisfactory. Therefore, better formulations/carriers are necessary to address the limitations. The first major challenge is the difficulties of developing drug carriers that encapsulate sufficient active therapeutic agents. Second, the toxicity of carrier materials remains a problem. Third, a prerequisite for clinical translocation and industrial production is the cost□effective and scalable fabrication of well□dispersed drug-loaded particles, which currently remains a great challenge. These barriers should be overcome to realize the clinical translocation of developed formulations. To overcome these limitation, I developed and evaluated two ophthalmic drug delivery systems using highly porous inorganic materials.

MOFs possess several potential advantages over existing nano- and micro-carriers. First, MOFs are structurally and compositionally diverse, allowing for the facile synthesis of MOFs of different sizes, shapes, compositions, and chemical properties. Second, MOFs are naturally biodegradable as a result of relatively labile metal-ligand bonds (covalent or coordination bond), making it possible for them to rapidly degrade in physiological conditions and clear the particles after

the intended work is completed. Among the various MOFs, MOFs composed of iron ions and ligands with appropriate surface−charge for drug loading were selected, synthesized and applied to the drug delivery systems to deliver ophthalmic drugs. This work will be presented in Chapter 2.

In addition, among inorganic biocompatible materials, mesoporous silica microparticles have a tailorable mesoporous structure, large pore volume and high specific surface area. These properties enable them to encapsulate a variety of therapeutic agents and deliver these active agents to the site of interest. Importantly, the fabrication of MSNs is simple, cost☐ effective, scalable, and controllable. Being abundantly distributed in nature, silicas have good compatibility and are accepted as "Generally Recognized As Safe" (GRAS) by the FDA and have been widely used in cosmetics and as FDA☐ approved food additives [38, 47]. In this regard, I synthesized SBA−15 mesoporous silica microparticles and grafted their surface using amino−silane to add mucoadhesive properties. The prepared particles were loaded on dexamethasone and applied to an inflammation − inhibiting drug delivery system for eyeballs then evaluated for mucoadhesion *in vitro* and *in vivo*. This work will be presented in Chapter 3.

Chapter 2

Metal-organic frameworks, NH$_2$-MIL-88(Fe), as carriers for ophthalmic delivery of brimonidine

2.1 Introduction

Metal-organic frameworks (MOFs) are crystalline inorganicorganic hybrid materials composed of metal ions or clusters as the coordination center and multidentate bridging

organic linkers interconnected between the metal nodes in one-, two-, or three-dimensional networks [14, 48]. MOFs have exceptionally large internal surface areas with uniform pores (up to 6500 m^2). They have large pore volumes (up to 2 cm^3/g) and exhibit various properties (e.g., topology, pore size, and total pore volume) that can be readily tuned by varying the molecular building blocks [13, 49]; additionally, their surfaces can be easily functionalized under relatively mild conditions [50]. Therefore, MOFs have been proposed as promising materials for many different applications, such as adsorption [51], separation [52], catalysis [53], and gas storage [54].

More recently, MOFs, composed of biocompatible metal ions and organic ligands, have been studied for a wide range of potential biomedical applications [13, 26]. MOFs appear particularly suited to drug delivery carriers because they can effectively encapsulate drugs into their high pore volume and release drugs in a controlled manner through the adjustment of pore sizes. Thus, MOFs have been actively studied to validate their efficacy in *in vivo* settings [28].

Therefore, I have proposed a MOF, $NH_2-MIL-88(Fe)$, as a delivery vehicle for an ophthalmic drug. This specific MOF is

36

composed of a metal ion (Fe) with an organic ligand of 2-aminoterephthalic acid, which have been proven sufficiently biocompatible [13, 55].

Ophthalmic drugs are generally formulated as eye drops and administered topically to the eye because of the ease of administration and high patient acceptance [56, 57] . However, eye drops are eliminated very rapidly from the surface of the eye (<3 min), thereby limiting their ocular bioavailability (<5%) [58]. To compensate this, eye drops are prescribed at high doses or in high frequency dosing regimens, which may exacerbate side effects and reduce patient compliance [59]. Therefore, to improve the therapeutic benefits of these drugs, one strategy would be to prolong their retention in the preocular space, allowing sustained drug release and, consequently, higher drug absorption into the eye [60-62].

In this work, I synthesized $NH_2-MIL-88(Fe)$ [$Fe_3O(BDC-NH_2)_3$, with $BDC-NH_2$, also termed 2-aminoterephthalic acid], following the previous protocol [63], and evaluated its suitability as a carrier for topical drug delivery to the eye. I hypothesized that the $NH_2-MIL-88(Fe)$ particles function via the following process: first, NH_2-MIL-

88(Fe) possesses hydrogen-rich organic ligands and amino groups, which can form hydrogen bonds with the intrinsic carboxyl and hydroxyl groups of mucin, respectively. Thus, the hydrogen bonding generates a mucoadhesive property to increase the preocular retention of NH_2-MIL-88(Fe) particles. Moreover, this effect can be promoted by the inherent high specific surface area, i.e., the vast number of surface amino groups of the NH_2-MIL-88 (Fe) [64]. With a longer retention on the preocular surface, the NH_2-MIL-88(Fe) particles can release the loaded drug in a sustained manner; it is found in tears for a prolonged period, which improves drug absorption into the eye.

To test this hypothesis, I used brimonidine, an anti-glaucoma medication, as a model ophthalmic drug. Brimonidine is a clinically-approved medication to reduce intraocular pressure in patients with glaucoma; however, when administered in the form of eye drops, it is recommended to be administered more than three times per day because of rapid preocular clearance and the resulting low ocular drug bioavailability [65]. In this study, NH_2-MIL-88(Fe) was synthesized by a previously reported solvothermal method [63]

and the reproducibility of the particles herein was confirmed by powder X-ray diffraction (XRD), Fourier transform infrared (FTIR) analysis, thermogravimetric analysis (TGA), electron microscopy, and N_2 adsorption-desorption measurements. Brimonidine was then encapsulated in NH_2-MIL-88(Fe) via physical adsorption and the drug-loaded NH_2-MIL-88(Fe) was assessed for mucoadhesion, cytotoxicity, and release behaviors in *in vitro* environments. In addition, *in vivo* evaluations in rabbit eyes were performed to examine the preocular retention property, drug bioavailability, and the period of efficacy after topical administration of the brimonidine-loaded particles of NH_2-MIL-88(Fe).

2.2 Materials and Methods

2.2.1 Materials

$FeCl_3 \cdot 6H_2O$ (98%), 2-aminoterephthalic acid (BDC-NH_2; Aldrich, 99%), N,N-dimethylformamide (DMF; Aldrich, anhydrous, 99.8%), ethanol (96%), acetic acid (99.7%), sodium acetate (99%), Schiff's fuchsin-sulfite reagent, and mucin

(Type I-S) were purchased from Sigma-Aldrich (USA). Brimonidine (assay >99.8%) and Alphagan P were supplied by Nanjing Yuance Industry & Trade (China) and Samil Allergan (Korea), respectively. Proparacaine hydrochloride (Alcaine®; 0.5% ophthalmic solution) was purchased from Alcon-Couvreur (Belgium).

2.2.2 Preparation of NH_2-MIL-88(Fe)

NH_2-MIL-88(Fe) was synthesized in accordance with a previously reported procedure with slight modifications (Scheme 1) [13, 63]. Briefly, 0.126 g (0.692 mmol) BDC-NH_2 and 0.187 g (0.692 mmol) $FeCl_3•6H_2O$ were dissolved in 15 mL DMF and the resulting mixture was vigorously stirred for 1 h. The substrate mixture was heated in a convection oven at 110 °C for 24 h in a Teflonlined autoclave to cause crystallization. After cooling to ambient temperature, the solid brown product was collected and washed with DMF and ethanol to remove excess reactants and yield NH_2-MIL-88(Fe) particles, which were dried at 100 °C overnight and soaked in ethanol at 80 °C for 24 h. Subsequently, the solvent was removed in a vacuum oven at 160 °C for 12 h and the resulting NH_2-MIL-88(Fe)

was sterilized with ethylene oxide prior to *in vitro* and *in vivo* evaluations.

To encapsulate brimonidine into the porous $NH_2-MIL-88(Fe)$ (i.e., $NH_2-MIL-88(Fe)/Br$), 50 mg brimonidine was first dissolved in 5 mL deionized (DI) water. To this solution, 200 mg $NH_2-MIL-88(Fe)$ was added with continuous stirring at 100 rpm for 24 h. Next, the suspension was filtered through a 200-nm polytetrafluoroethylene membrane filter (Hyundai Micro, Korea) to obtain $NH_2-MIL-88(Fe)/Br$, which was washed with ethanol three times. To calculate the amount of brimonidine that was loaded in $NH_2-MIL-88(Fe)$, the concentration of brimonidine measured after the loading procedure was subtracted from the known initial concentration of the brimonidine. The concentration of brimonidine was measured by using high-performance liquid chromatography (HPLC; Agilent 1260 series, Agilent Technologies, USA) using a Diamonsil C18 column (150 x 4.6 mm, 5 mm; Dikma Technologies, USA) [66]. The mobile phase was a mixture of 20 mM phosphatebuffered saline (PBS; pH 2.5) and acetonitrile (88:12, v/v). The flow rate and injection volume were 1 mL/min and 10 mL, respectively. The column temperature was

maintained at 37 ℃ and absorbance was measured at 248 nm. Through the use of these analytical methods, the drug concentrations were analyzed in the range from 10 to 500 mg/mL with a standard curve with R^2 > 0.999.
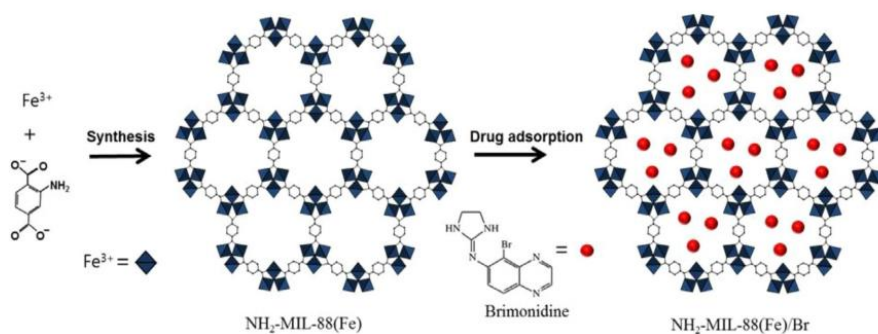
Figure 2.1. Schematic illustration of the synthesis of $NH_2-MIL-88(Fe)$ and the encapsulation of brimonidine in $NH_2-MIL-88(Fe)$ (i.e., $NH_2-MIL-88(Fe)/Br$).

2.2.3 Characterizations

The X-ray powder diffraction (XRD; D/Max 2200, Rigaku, Tokyo, Japan) patterns of $NH_2-MIL-88(Fe)$ and $NH_2-MIL-88(Fe)/Br$ were measured by using Ni-filtered Cu-Ka radiation (k = 1.5418 Å) at 0.5°/min. The samples were loaded onto glass holders and continuously scanned with a tube voltage of 40 kV and current of 30 mA. The FTIR spectra of $NH_2-MIL-88(Fe)$, brimonidine, and $NH_2-MIL-88(Fe)/Br$ were obtained by using a JASCO 6100 (JASCO, Japan) spectrophotometer over the range of 4000–400 cm^{-1} with a 4 cm^{-1} resolution at room temperature (i.e., 25 °C). A TGA curve was also recorded by using a thermogravimetric analyzer (Q50; TA Instrument, USA). For this experiment, approximately 10 mg sample was loaded, and the temperature was increased from room temperature to 900 °C at a rate of 10 °C /min under a N_2 flow rate of 50 mL/min. The surface area, pore size, and pore volume were determined by using a surface area and porosity analyzer (ASAP 2020; Micromeritics, USA) at −196 °C. Prior to measurements, samples were degassed at 120 °C for 6 h under vacuum conditions. The size and morphology of $NH_2-MIL-88(Fe)$ were evaluated by using a scanning electron

microscope (SEM; JEOL-7800F, JEOL, Japan).

To examine the *in vitro* drug release profiles, 10 mg NH_2-MIL-88(Fe)/Br was added to 10 mL PBS (pH 7.4). Then, the particle suspension was incubated in a shaking incubator (SI-600R; Jeio Tech, Seoul, Korea) at 37 °C with continuous stirring at 125 rpm. At predetermined times, 1 mL release medium was collected and an equal volume of fresh buffer was added to the medium. The concentration of brimonidine in the sampled aliquots was assayed by using the HPLC method described above.

2.2.4 *In vitro* cytotoxicity evaluation

To evaluate the cytotoxicity of NH_2-MIL-88(Fe) and NH_2-MIL-88(Fe)/Br, I performed a cell viability assay in human primary corneal epithelial cells (PCS-700–010, ATCC, USA) [67, 68]. The corneal epithelial cells were grown in corneal epithelial cell basal medium (PCS-700-030, ATCC, USA) supplemented with a corneal epithelial cell growth kit (PCS-700-040, ATCC, USA) at 37 °C in a humidified atmosphere with 5% CO_2.

I used an extraction method to examine the cytotoxicity of

NH$_2$-MIL-88(Fe) and NH$_2$-MIL-88(Fe)/Br. First, NH$_2$-MIL-88(Fe) and/or NH$_2$-MIL-88(Fe)/Br was suspended in the cell growth medium at concentrations between 5 and 2000 mg/mL and incubated with continuous agitation (125 rpm) at 37 ℃ (SI-600R, Jeio Tech, Korea) for 24 h. The extracted media were used to evaluate cell viability(Ez-Cytox; Daeil Lab Service, Seoul, Korea) in accordance with the manufacturer's instructions. In brief, corneal epithelial cells were seeded in 24-well culture plates at an initial density of 1 x 10^5 cells/well and grown for 24 h. Subsequently, the media were completely replaced with extracted media and cells were incubated for another 24 h. The cell media were mixed with 50 mL Ez-Cytox solution, incubated in the dark for 2 h, and the absorbance was measured at 450 nm against a reference wavelength of 600 nm (VersaMax ELISA Microplate Reader; Molecular Devices, Sunnyvale, CA, USA).

2.2.5 *In vitro* evaluation of mucoadhesive property

I evaluated the mucoadhesive properties of NH$_2$-MIL-88(Fe) and NH$_2$-MIL-88(Fe)/Br in two separate assays. First, I measured the changes in the surface charge of the particles

before and after interaction with mucin. This was evaluated through measurement of the zeta potential of the particles was by using a Zeta Sizer (ELS-2000ZS, Otsuka Electronics, Japan) before and after the particles (2 mg) were incubated in 2 mL of a Type I-S mucin solution (1 mg/mL in 10^{-3} M KCl solution) for 1 h [69]. As a control, the zeta potential of mucin itself was also measured. Second, I measured the amount of mucin that was adsorbed onto NH_2-MIL-88(Fe)/Br. For this, I dispersed 4 mg NH_2-MIL-88(Fe)/Br in 2 mL Type I-S mucin solution (1 mg/mL in DI water), which was then incubated at 37 °C for 0.5, 1, 2, and 6 h, respectively. Subsequently, suspensions were centrifuged (10,000xg for 10 min) and the remaining free mucin in the supernatant was measured spectrophotometrically in accordance with the periodic acid/Schiff (PAS) colorimetric method [70, 71]. To calculate the amount of mucin that was adsorbed to NH_2-MIL-88(Fe)/Br, the amount of free mucin remaining in the supernatant was subtracted from the amount of mucin that was initially added to the solution.

2.2.6 Animal experiments

In vivo experiments were conducted on healthy male New

Zealand White rabbits (weight: 3–4 kg; Cheonam Yonam College, Chungcheonagnam—do, Korea). The experimental protocol was approved by the Institutional Animal Care and Use Committee at the Biomedical Research Institute of the Seoul National University Hospital (IACUC No. 13—0101). The rabbits were housed in separate cages and maintained in a controlled environment (temperature, 21 ± 1 °C; humidity, $55\% \pm 1\%$; 12 h/12 h light/dark cycle). Food and water were provided to the rabbits ad libitum. *In vivo* experiments herein were performed at 7 am–7 pm.

In vivo preocular retention of $NH_2-MIL-88(Fe)/Br$ was evaluated by following a previously reported protocol, with slight modifications [72, 73]. Approximately 0.433 mg $NH_2-MIL-88(Fe)/Br$ was suspended in 35 μL PBS, which was administered into the lower cul—de—sac of the rabbit eye without anesthesia while the rabbit was positioned in a restriction bag with only its head exposed. At scheduled times after administration, the eye was locally anesthetized by using a drop (35 μL) of Alcaine® and the remaining $NH_2-MIL-88(Fe)/Br$ particles were completely wiped from the eye by using a surgical sponge (PVA Spears; Network Medical

Products, UK). The sponge with the particles was completely dissolved in nitric acid and the resulting solution was analyzed by using inductively coupled plasma-mass spectroscopy (ICP-MS; NexION 350D, Perkin-Elmer, MA, USA) to quantify the Fe ion. The measured amount of Fe ion was then divided by the amount of Fe ion of the initially administered NH_2-MIL-88(Fe)/Br (0.433 mg) to determine the percentage of the particles remaining in the preocular space. For this experiment, four animals (i.e., one left eye for each animal) were assigned at each time of measurement. To evaluate the *in vivo* drug delivery efficacy, the intraocular pressure (IOP) was measured after topical administration of NH_2-MIL-88(Fe)/Br to the eye and compared with that after the administration of Alphagan P [65]. The rabbit eyes were locally anesthetized with a drop of 35 μL Alcaine® and after 2–3 min, the IOP was measured with a tonometer (Tono-Pen AVIA; Reichert, USA).

Before administration, the baseline IOP ($IOP_{baseline}$) of each rabbit was measured. Afterwards, a 35 μL drop of NH_2-MIL-88(Fe)/Br suspension or Alphagan P, in which each formulation contained the same dose (52.5 μg) of brimonidine, was administered into the lower cul-de-sac of the rabbit eye.

The IOP ($IOP_{scheduled\ time}$) was then measured at predetermined time points (1, 2, 4, 6, 8, 10, and 12 h) after administration. The change in IOP was calculated from the following equation:

$$\% \text{ Change in IOP} = \frac{IOP_{baseline} - IOP_{scheduled\ time}}{IOP_{baseline}}$$

For this IOP measurement, four animals (i.e., one left eye for each animal) were assigned for each type of the tested formulations.

I also measured the amount of drug that was absorbed into the eye with $NH_2-MIL-88(Fe)/Br$ and compared this value with that of Alphagan P. For this, the brimonidine formulation (i.e., the $NH_2-MIL-88(Fe)/Br$ suspension or Alphagan P) was administered in the lower cul-de-sac of the rabbit eye, as described above. At scheduled time points after administration, the rabbit was anesthetized with an intramuscular injection of a cocktail of 17.5 mg/kg ketamine and 5 mg/kg xylazine. After local anesthesia of the eye with a drop of 35 μL Alcaine®, ~100 μL of the aqueous humor (AH) was aspirated by using a 30-gauge disposal needle. For each type of the tested formulations, four animals (i.e., one left eye for each animal) were assigned at each time of measurement. The concentration of brimonidine from the sample was determined by using a HPLC-mass

50

spectrometer (LC–MS; Agilent 6120 Series Quadrupole LC/MS, Agilent Technologies, USA) using a InfinityLab Poroshell column (120 EC–C18, 4.6 x 50 mm, 2.7 lm pore size, Agilent Technologies, CA, USA). The mobile phase was composed of 0.1% formic acid and acetonitrile (90:10, v/v). The flow rate and sample injection volume were 0.5 mL/min and 10 μL, respectively. The column temperature was maintained at 30 °C and detection mass ion was 294 [M+2]. The collected aqueous humor samples were analyzed without further treatment. The standard curve of 5, 10, 50, 100, 500, and 1000 ng/mL brimonidine solution was prepared.

I also sought to compare the drug efficacy of a single administration of NH_2–MIL–88(Fe)/Br with those of multiple administrations of Alphagan P. To examine the effect of the dose amount, Alphagan P was administered two, three, or four times in a row with an interval of 1 min; this produced the animal treatment groups of Alphagan P (2X), Alphagan P (3X), or Alphagan P (4X), respectively. To assess the effect of the dosing schedules, Alphagan P was also administered 1, 3, or 5 h after the first administration; this produced the animal treatment groups of Alphagan P (1 h), Alphagan P (3 h), or

Alphagan P (5 h), respectively. For all the animal groups above, the change in IOP was measured at the scheduled times of 1, 2, 4, 6, 8, 10, and 12 h after the first administration of Alphagan P, as described above. At each time of measurements, four and five animals (i.e., one left eye for each animal) were assigned for Alphagan P and $NH_2-MIL-88(Fe)/Br$, respectively.

2.2.7 *In vivo* safety evaluation

To evaluate the safety of $NH_2-MIL-88(Fe)/Br$, two different experiments were conducted by an ophthalmologist in a blinded manner. First, the eye was visually examined 24 h after a single administration of the $NH_2-MIL-88(Fe)/Br$ suspension. For a longer-term evaluation, I administered a drop of the $NH_2-MIL- 88(Fe)/Br$ suspension twice per day for 7 days (i.e., a total of 14 administrations). On the last day of experiments, the eye was stained with 5 μL of a fluorescein sodium solution (0.25% w/v) and examined [74]. For each experiment, three animals (i.e., one left eye for each animal) were assigned and the examinations were performed after the rabbits were sedated by an intramuscular injection of a cocktail of 17.5 mg/kg ketamine and 5 mg/kg xylazine.

2.2.8 Statistical analysis

The mean change in IOP and brimonidine concentration in AH were statistically analyzed using Mann-Whitney U test, where $p < 0.05$ was considered to indicate a statistically significant difference between the values after $NH_2-MIL-88(Fe)/Br$ and Alphagan P administration at each time point (SPSS version 22, IBM, USA).

2.3 Results

2.3.1 Particle characterization

After the synthesis, the $NH_2-MIL-88(Fe)$ particles were characterized. The XRD analysis indicated that the characteristic peaks originating from the well-known crystalline structure of $NH_2-MIL-88(Fe)$ were clearly observed in both $NH_2-MIL-88(Fe)$ and $NH_2-MIL-88(Fe)/Br$ (Figure. 2.2) [63, 75]. This result suggested that the physical absorption of brimonidine did not influence the major structure of $NH_2-MIL-88(Fe)$. I also examined the FTIR spectra of $NH_2-MIL-88(Fe)$, brimonidine, and $NH_2-MIL-88(Fe)/Br$, as

shown in Figure. 2.3 NH$_2$−MIL−88(Fe) exhibited characteristic peaks at 3200–3500 cm^{-1} and 1656 cm^{-1} that were attributable to the primary amine (R−NH$_2$) and C=O groups, respectively [75]. Brimonidine exhibited characteristic peaks at 3212 and 3268 cm^{-1} owing to N–H stretching from the secondary amine group (RR'–NH) [76]. For NH$_2$−MIL−88(Fe)/Br, the characteristic bands from both NH$_2$−MIL−88(Fe) and brimonidine overlapped without any apparent shift, which implied that the chemical structures of NH$_2$−MIL−88(Fe) and brimonidine were not altered during the drug encapsulation process employed in this study. The loaded amount of brimonidine was measured as 121.3 mg/mg NH$_2$−MIL−88(Fe).

Next, I performed TGA on the dry powders of NH$_2$−MIL−88(Fe) and NH$_2$−MIL−88(Fe)/Br (Figure. 2.4). For the intact NH$_2$−MIL−88(Fe) without brimonidine, an initial weight loss occurred at −80 ℃, which was attributed to the removal/evaporation of the ethanol used as a washing solvent. The second weight loss at 200–480 ℃ was attributable to the structural collapse of the MOF, as previously reported [13]. For the NH$_2$−MIL−88(Fe)/Br, as well as those two weight losses, another distinct weight loss was observed at 490–640 °

54

C, which was ascribed to the loss of brimonidine (b.p. = 432.6 °C).

The N_2 adsorption-desorption isotherms of NH_2-MIL-88(Fe) and NH_2-MIL-88(Fe)/Br are shown in Figure. 2.5. NH_2-MIL-88(Fe) exhibited type IV pattern isotherms with an apparent hysteresis loop. As calculated using the Brunauer-Emmett-Teller (BET) method, the surface area and total pore volume of NH_2-MIL-88(Fe) were 992 m^2/g and 0.66 cm^3/g, respectively, which were in good agreement with a previous report [77]. In contrast, after drug loading, the NH_2-MIL-88(Fe)/Br exhibited isotherms with a less distinct hysteresis loop, resulting in a surface area and total pore volume of 105 m^2/g and 0.32 cm^3/g, respectively. The reduction in surface area and total pore volume could be ascribed to the presence of the encapsulated molecules of brimonidine in the pores of NH_2-MIL-88(Fe). The pore size distributions of NH_2-MIL-88(Fe) and NH_2-MIL-88(Fe)/Br were calculated by using the Barrett-Joyner-Halenda (BJH) method, which yielded size estimates of 9.6 and 5.2 Å, respectively, with a narrow distribution. Similarly, the pore size decreased in NH_2-MIL-88(Fe)/Br, possibly as a consequence of the encapsulated

55

brimonidine. The SEM images of $NH_2-MIL-88(Fe)$ and $NH_2-MIL-88$ (Fe)/Br, both of which exhibited sharp-ended rod-like shapes of 0.5–3 mm [13], are shown in Figure. 2.6.

Next, I performed an *in vitro* drug release experiment in PBS (pH 7.4), as shown in Figure. 2.7. After an initial burst release of approximately 40% brimonidine during the first 30 min, the $NH_2-MIL-88(Fe)/Br$ exhibited a sustained drug release pattern for 12 h with an average release rate of 5.2%/h, which could be more sustained *in vivo* as the volume of tear fluid (~8 μL) [78] is much lower than that used for *in vitro* drug release study herein (10 mL). The burst release was attributable to the water-soluble drug molecules distributed on the surface of $NH_2-MIL-88(Fe)$ [79] while sustained drug release afterwards could be ascribed to drug diffusion via the pores and carrier degradation (Figure. 2.8).
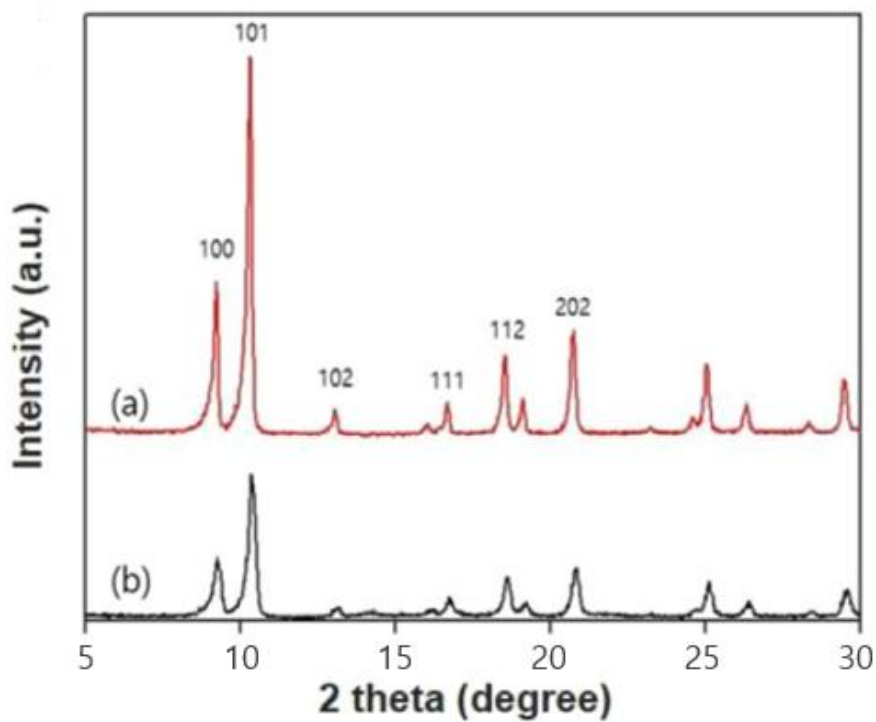
Figure 2.2. Powder X−ray diffraction patterns of (a) NH_2−MIL−88(Fe) and (b) NH_2−MIL−88(Fe)/Br.
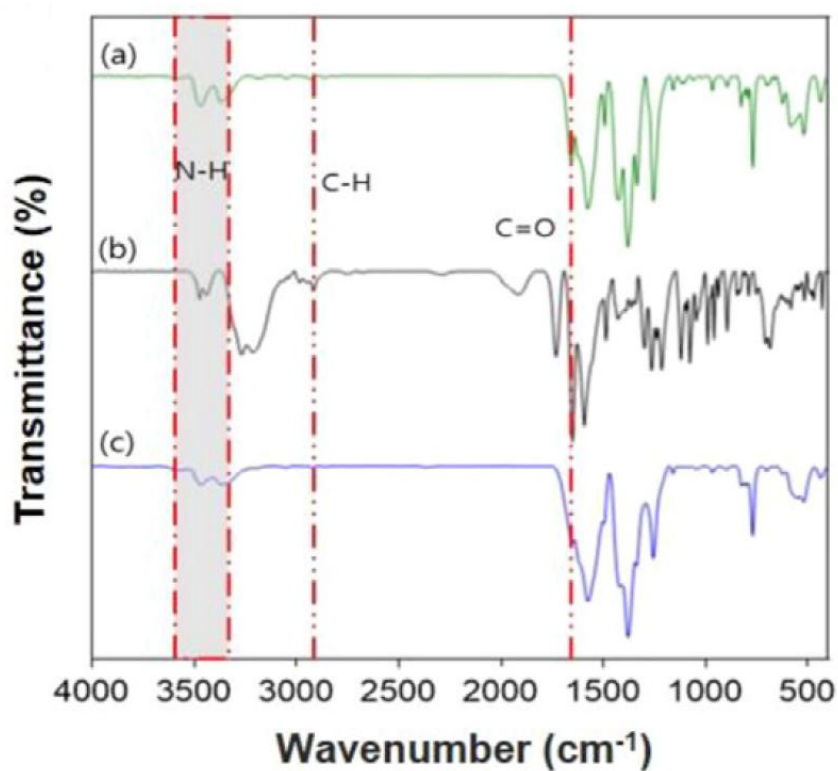
Figure 2.3. Infrared spectra of (a) $NH_2-MIL-88(Fe)$, (b) brimonidine and (c) $NH_2-MIL-88(Fe)/Br$.
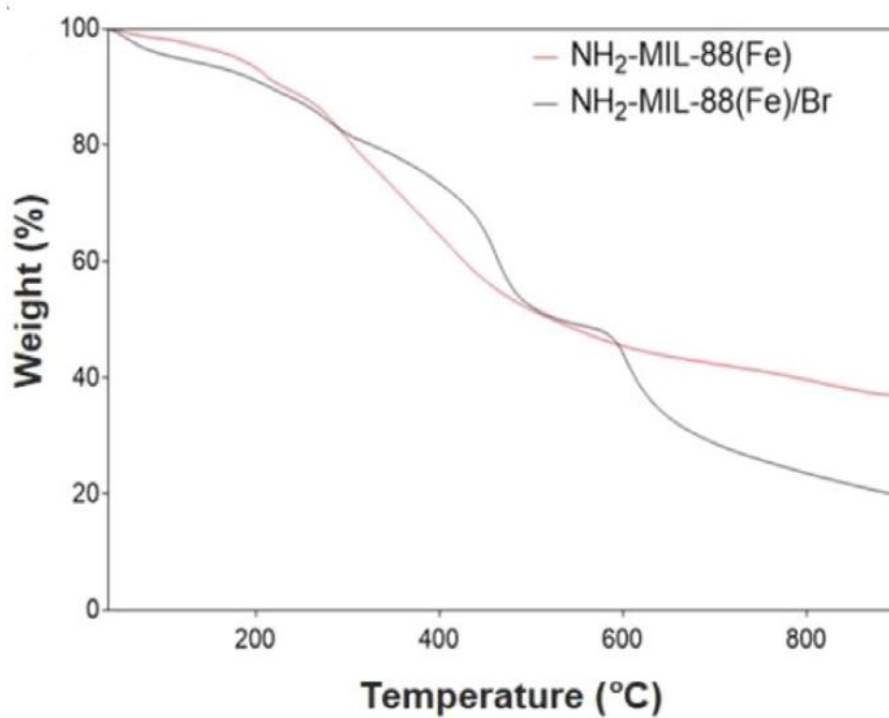
Figure 2.4. Thermogravimetric curves for $NH_2-MIL-88(Fe)$ and $NH_2-MIL-88(Fe)/Br$.
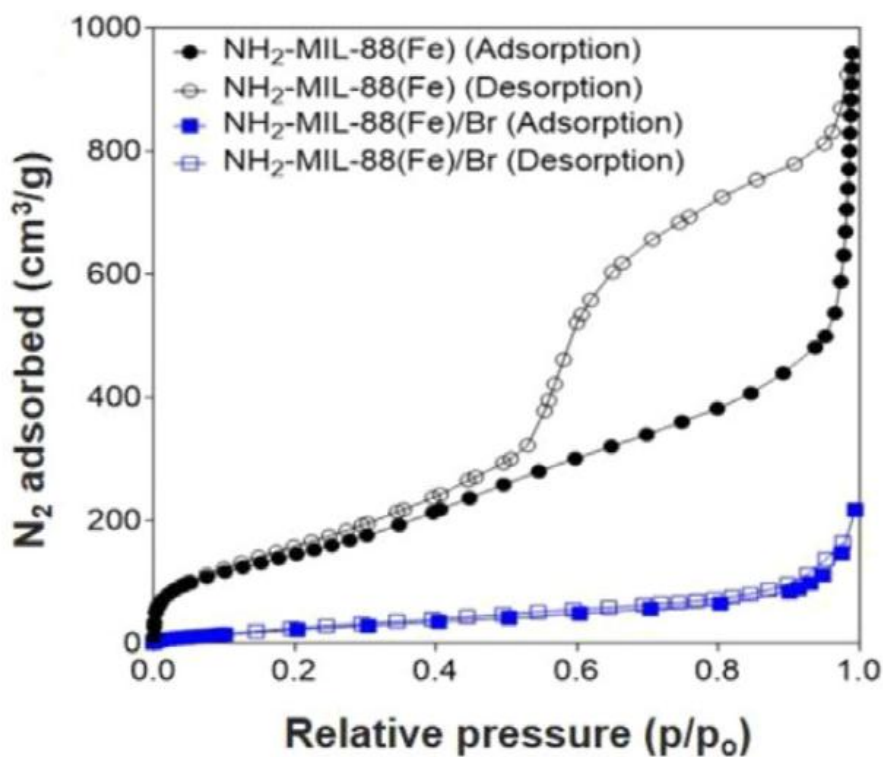
Figure 2.5. N_2 isotherm profiles of (a) $NH_2-MIL-88(Fe)$ and (b) $NH_2-MIL-88(Fe)/Br$ at 77 K. Closed symbols indicate adsorption; open symbols indicate desorption.
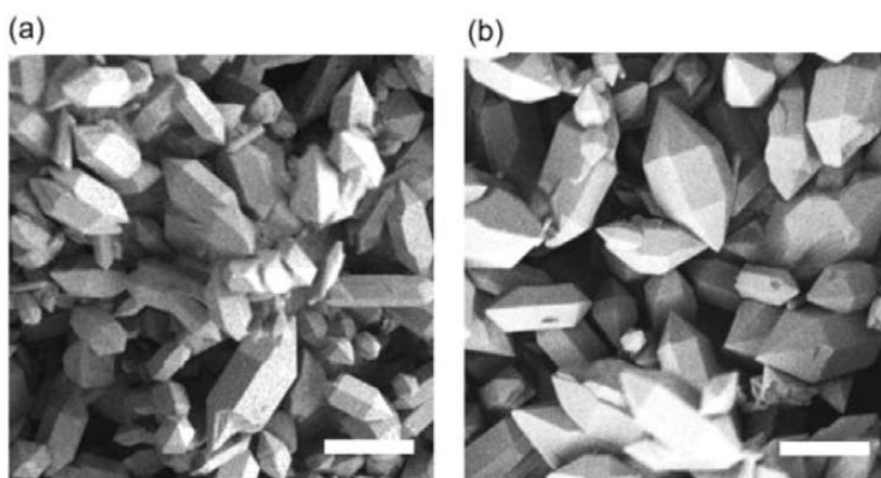
Figure 2.6. Representative scanning electron micrographs of (a) NH$_2$−MIL−88(Fe) and (b) NH$_2$−MIL−88(Fe)/Br; scale bar = 2 mm.
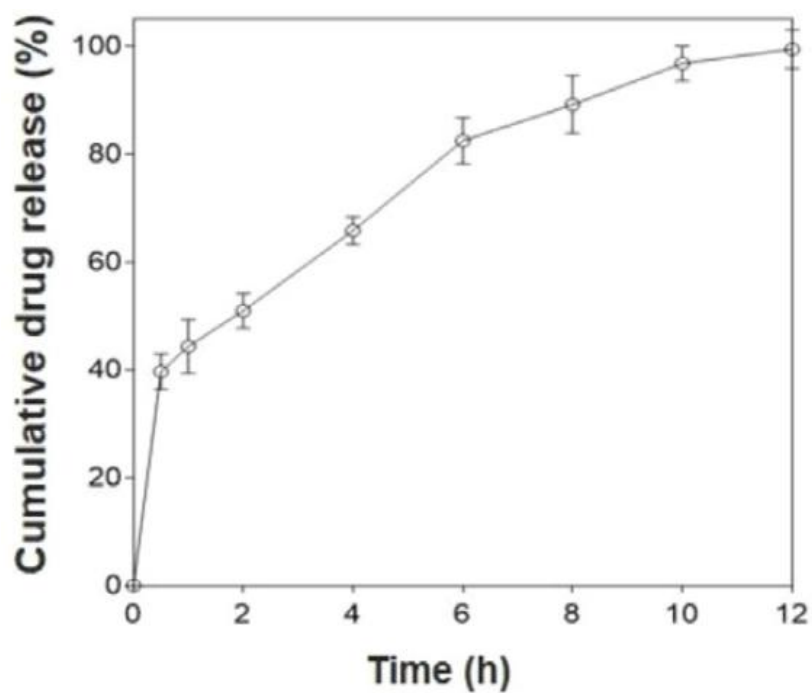
Figure 2.7. *In vitro* release profile of brimonidine from NH_2-MIL-88(Fe)/Br in PBS (pH 7.4). Error bars = ± SD (n =3).
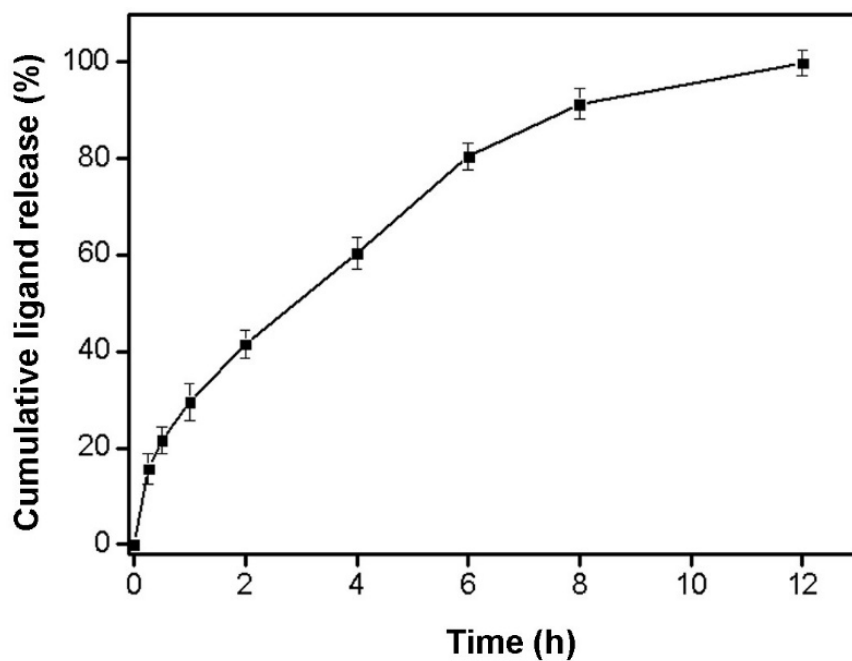
Figure 2.8. *In vitro* degradation profile of $NH_2-MIL-88(Fe)/Br$ in pH 7.4 PBS, showing almost 100% degradation in 12 h. Error bars = ± SD (n =3).

2.3.2 Cytotoxicity

I evaluated the cytotoxicity of $NH_2-MIL-88(Fe)$ and $NH_2-MIL-88(Fe)/Br$ in HCE cells. As shown in Figure. 2.9, the growth of HCE cells was not markedly affected by the extract from the suspension of $NH_2-MIL-88(Fe)$ and $NH_2-MIL-88(Fe)/Br$, even at high concentrations (i.e., 2000 mg/mL). This finding suggested that the $NH_2-MIL-88(Fe)/Br$ prepared in this study was not cytotoxic.

(A)

(B)
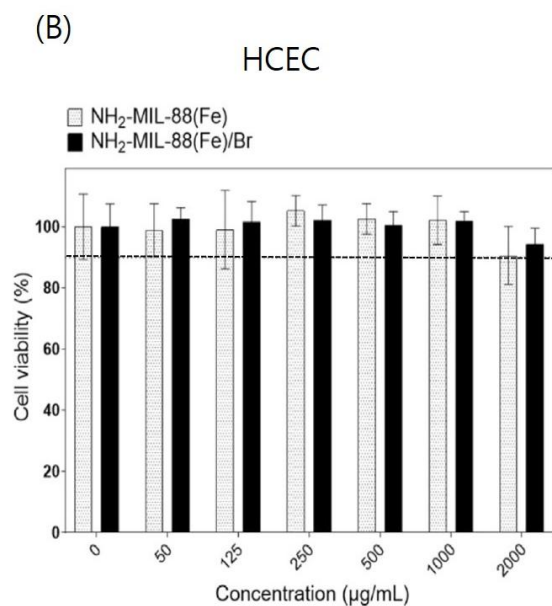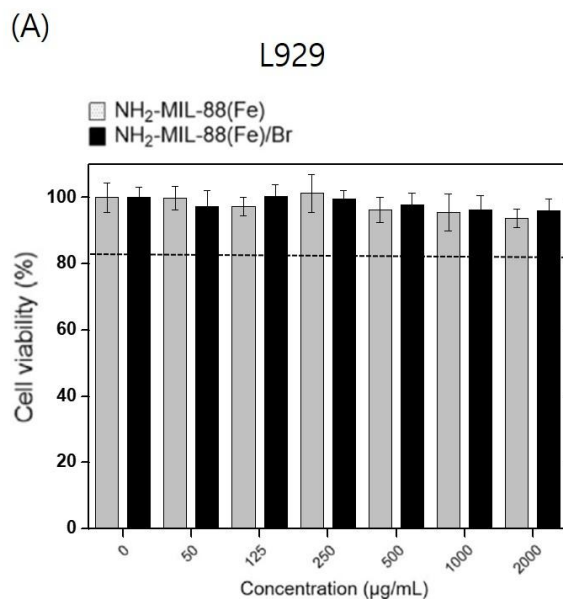
Figure 2.9. *In vitro* cytotoxicity of $NH_2-MIL-88(Fe)$ (grey) and $NH_2-MIL-88(Fe)/Br$ (black) assessed on (A) L929 and (B) human primary corneal epithelial cells (HCEC). Error bars = ± SD (n =8).

2.3.3 Mucoadhesive property

To assess the mucoadhesive properties, I measured the change in surface charge of $NH_2-MIL-88(Fe)$ and $NH_2-MIL-88(Fe)/Br$ before and after interaction with mucin. As shown in Figure. 2.10, mucin itself has a negative zeta-potential of -30.99 mV [69]. $NH_2-MIL-88(Fe)$ had a positive zeta-potential, 4.01 mV, owing to the presence of amino groups; however, after the loading of an anionic drug, brimonidine, the zeta potential of $NH_2-MIL-88(Fe)/Br$ was shifted to -9.90 mV. After interaction with mucin, it should be noted that the surface charges of both $NH_2-MIL-88(Fe)$ and $NH_2-MIL-88(Fe)/Br$ were shifted to more negative values of -23.25 mV and -18.8 mV, respectively, which could be ascribed to the surface-adhered mucin with a greater negative charge (-30.99 mV). I quantified the mucin adsorption (Figure. 2.11) and determined that the amount of mucin adsorbed onto $NH_2-MIL-88(Fe)$ was 342 ± 26 mg/mg after 30 min and increased to 398 ± 15 mg/mg after 1 h, which provided further evidence of the mucoadhesive property of $NH_2-MIL-88(Fe)/Br$. The resulting amounts of adhered mucin were comparable with those reported for a well-known mucoadhesive material, such as chitosan particles,

in a previous study [80].
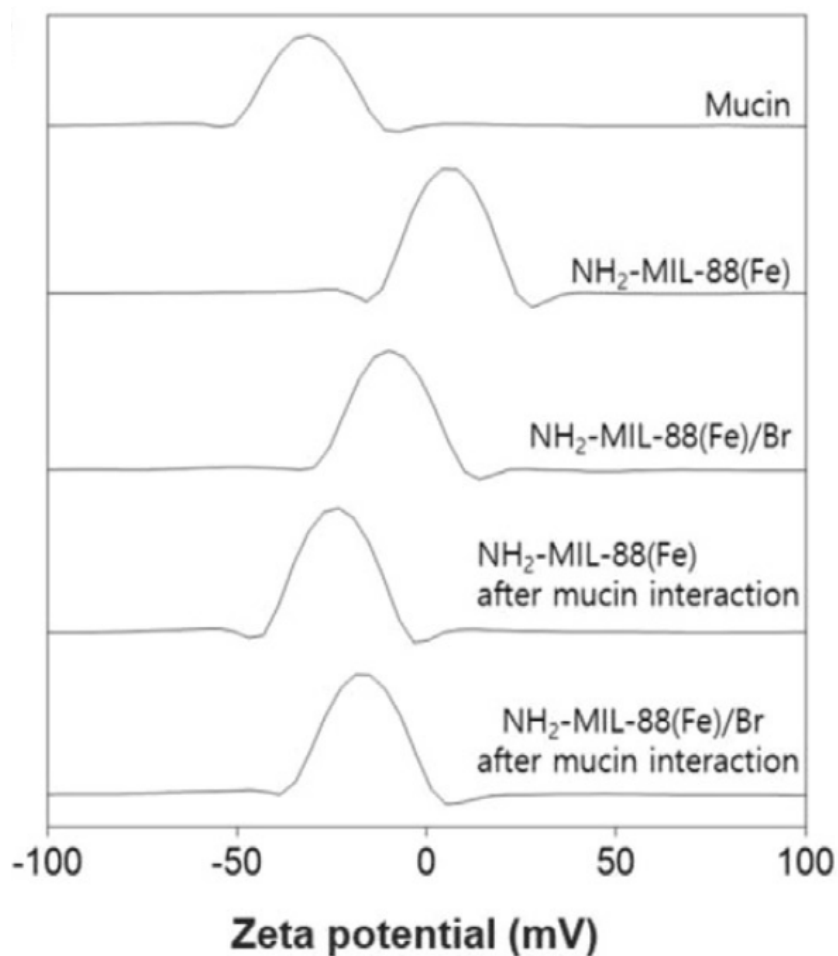
Figure 2.10. Zeta potential values obtained before and after the incubation of $NH_2-MIL-88(Fe)$ and $NH_2-MIL-88(Fe)/Br$ with mucin.
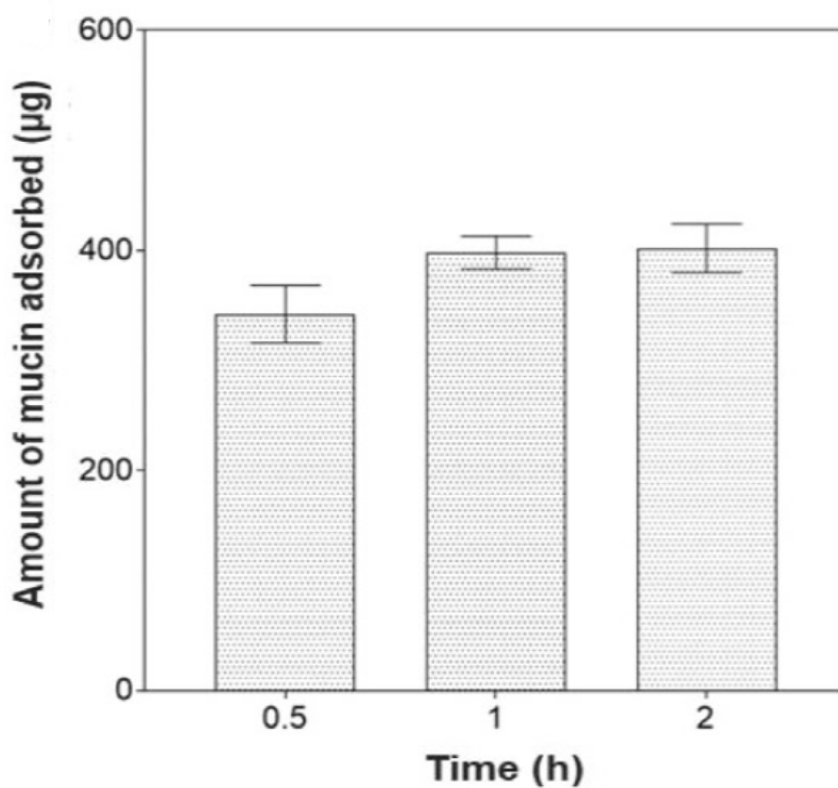
Figure 2.11. Amount of mucin adsorbed on $NH_2-MIL-88(Fe)/Br$ over time. Error bars $= \pm$ SD (n =3).

2.3.4 *In vivo* preocular retention property

To examine the preocular retention property, I measured the amount of the $NH_2-MIL-88(Fe)/Br$ remaining in the preocular space after the topical administration to rabbit eyes. As shown in Figure. 2.12, approximately 32.5% of $NH_2-MIL-88(Fe)/Br$ remained on the preocular surface at 30 min and more than 10.04% and 3.52% were present at 1 and 2 h, respectively. Compared with the residence time of the conventional eye drops, which was reported to be less than 3 min [81, 82], our findings suggested a prominent enhancement of the preocular retention property of $NH_2-MIL-88(Fe)/Br$, which could be a result of adhesion to the mucin present in the eye surface [2].
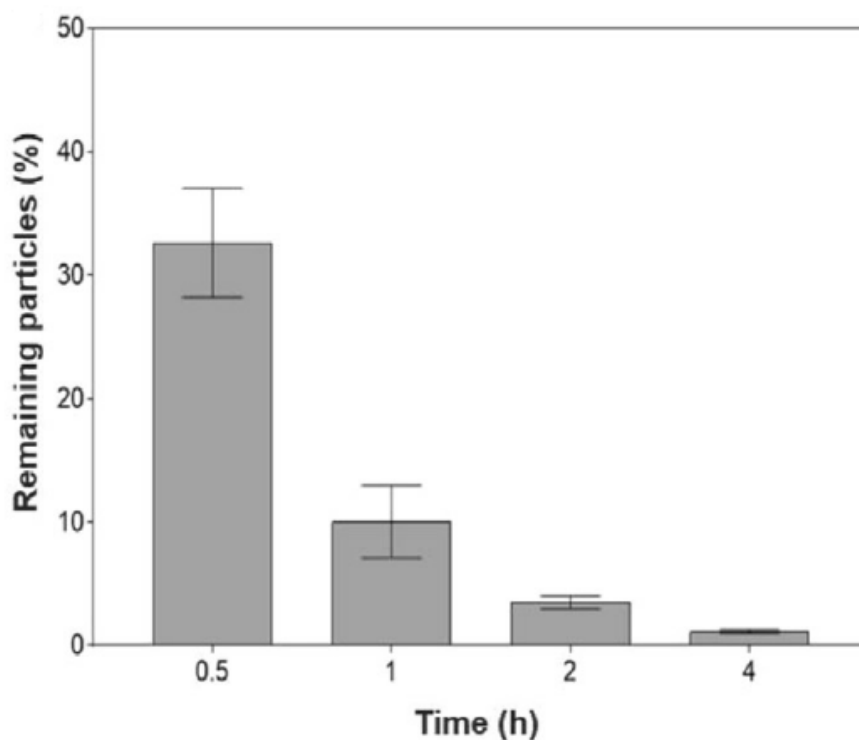
Figure 2.12. *In vivo* preocular retention profiles of $NH_2-MIL-88(Fe)/Br$ on rabbit eyes. The remaining percentage of $NH_2-MIL-88(Fe)/Br$ on the preocular surface was assessed by using ICP−MS at scheduled times after topical administration on the lower cul−de−sac. Error bars = ± SD (n =4).

2.3.5 *In vivo* drug efficacy

To examine the ocular drug efficacy, I measured the change in IOP after the administration of brimonidine formulations [65]. The brimonidine dose for a single administration was based on a single drop of Alphagan P, which is also prescribed in clinical settings [83]. As shown in Figure. 2.13, for Alphagan P, a decrease in IOP was observed for 6 h. In contrast, when the same dose of brimonidine was administered as $NH^2-MIL-88(Fe)/Br$, the period of IOP reduction persisted for 12 h, which was an increase of approximately two-fold. A slight delay in the maximum IOP reduction could potentially occur owing to the slow release of brimonidine; however, at 2 h, the mean IOP decrease was not significantly different between Alphagan P and $NH_2-MIL-88(Fe)/Br$. The percentage decrease of IOP with $NH_2-MIL-88(Fe)/Br$ was significantly higher than those with Alphagan P at 4, 6, 8, and 10 h ($p <$ 0.05).

For pharmacokinetic evaluation, I also measured the drug concentration in AH after the administration of the brimonidine formulations. As shown in Figure. 2.14 and Table 2.1, Alphagan P exhibited a peak drug concentration of 0.76

μg/mL at 1 h, which decreased relatively quickly and was undetectable at 6 h. In contrast, for $NH_2-MIL-88(Fe)/Br$, the peak drug level was measured as 0.73 μg/mL at 2 h, which decreased more slowly and was detectable until 10 h. Again, the peak drug concentration of $NH_2-MIL-88(Fe)/Br$ was probably observed slightly after that of Alphagan P because of the slow release of brimonidine. The drug concentration of $NH_2-MIL-88(Fe)/Br$ was significantly higher than that of Alphagan P at 2, 4, 6, 7, and 10 h ($p < 0.05$). Thus, as shown in Table 2.1, the half-life of brimonidine in $NH_2-MIL-88(Fe)/Br$ was calculated as 2.00 h, which was more than twice as long as that of Alphagan P (i.e., 0.92 h). When I compared the area under the drug concentration-time curve (AUC), a pharmacokinetic parameter that represents drug bioavailability, $NH_2-MIL-88(Fe)/Br$ also exhibited an increase of approximately two-fold when compared with Alphagan P.

For the consideration of the dose amount and regimen, I also compared the changes in IOP after a single administration of $NH_2-MIL-88(Fe)/Br$ with those of multiple administrations of Alphagan P. Thus, I first increased the dose of brimonidine by consecutive, multiple administrations of Alphagan P and

measured the IOP over time. As shown in Figure. 2.15, the period of IOP decrease was extended as the dose of Alphagan P increased. However, to be as effective as a single administration of $NH_2-MIL-88(Fe)/Br$, I determined that at least a four-fold higher dose of Alphagan P was needed (i.e., Alphagan P (4x)), which showed a period of IOP decrease of 12 h. Through the evaluation of the dosing schedules of Alphagan P (Figure. 2.16), the period of the IOP decrease could be extended up to 12 h with two-time administrations with an interval of 5 h (i.e., Alphagan P (5 h)); however, unlike the IOP profile of the $NH_2-MIL-88(Fe)/Br$, a prominent drop in IOP decrease was observed at 4 h.

Table 2.1 Pharmacokinetic parameters of brimonidine in aqueous humor after the administration of various formulations.

Formulation	C_{max} (μg mL^{-1})	T_{max} (h)	AUC (μg h mL^{-1})	Half-life (h)
Alphagan P	0.76	1	1.62	0.92
NH$_2$-MIL-88(Fe)/Br	0.73	2	3.23	2.00
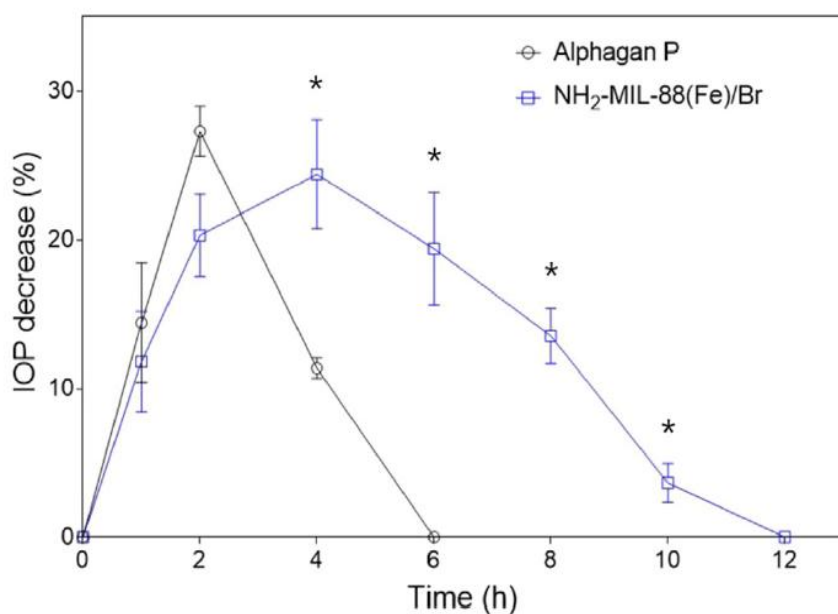
Figure 2.13. Percentage reduction in intraocular pressure (IOP) over time after the administration of Alphagan P and $NH_2-MIL-88(Fe)/Br$. *At 4, 6, 8, and 10 h, the effect of $NH_2-MIL-88(Fe)/Br$ was significantly different from that of Alphagan P. Error bars = ± SD (n =4).
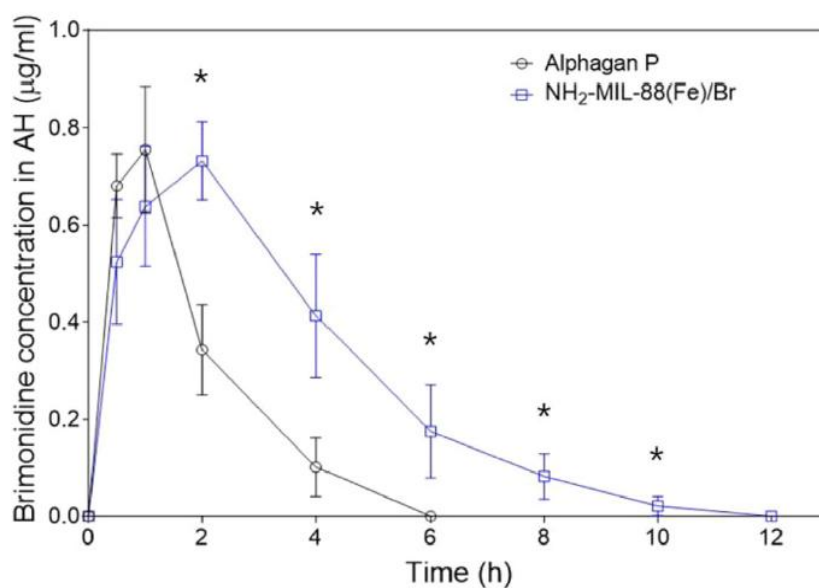
Figure 2.14. Brimonidine concentration in aqueous humor over time after the administration of Alphagan P and $NH_2-MIL-88(Fe)/Br$. *At 2, 4, 6, 8, 10 h, the effect of $NH_2-MIL-88(Fe)/Br$ was significantly different from that of Alphagan P. Error bars = ± SD (n =4).
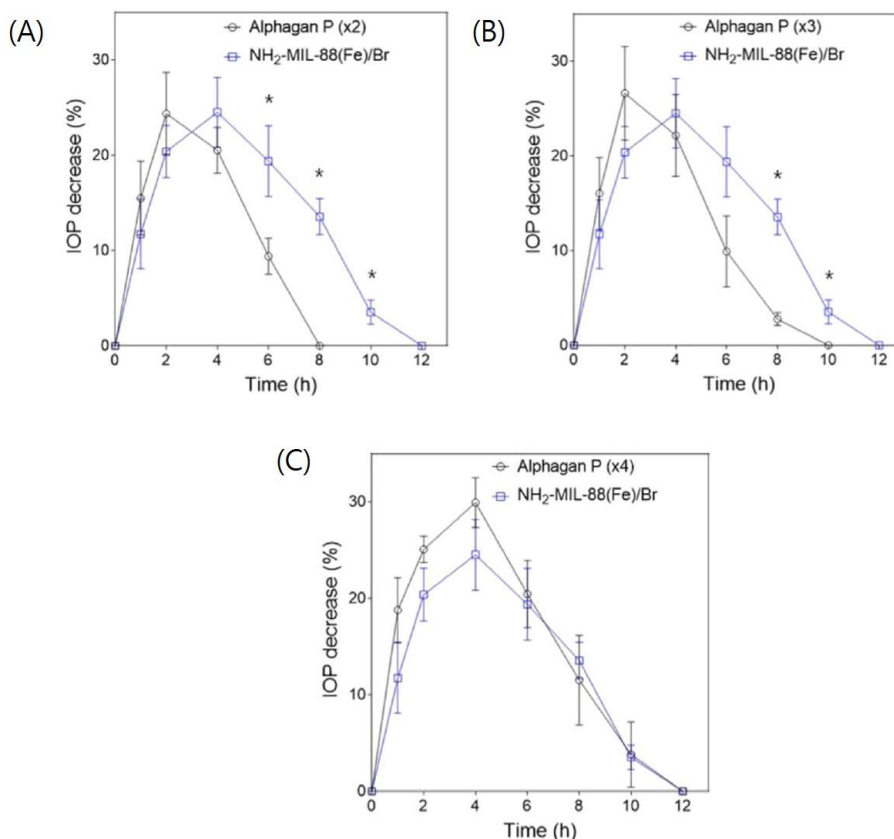
Figure 2.15. Percentage reduction in intraocular pressure (IOP) over time obtained from different Alphagan P administration protocols. The IOP profile was compared with that of $NH_2-MIL-88(Fe)/Br$. (A) Alphagan P (x2), (B) Alphagan P (x3), or (C) Alphagan (x4) was obtained with two, three, or four consecutive administrations of Alphagan P with 1 min intervals. Error bars = ± SD (n = 4).
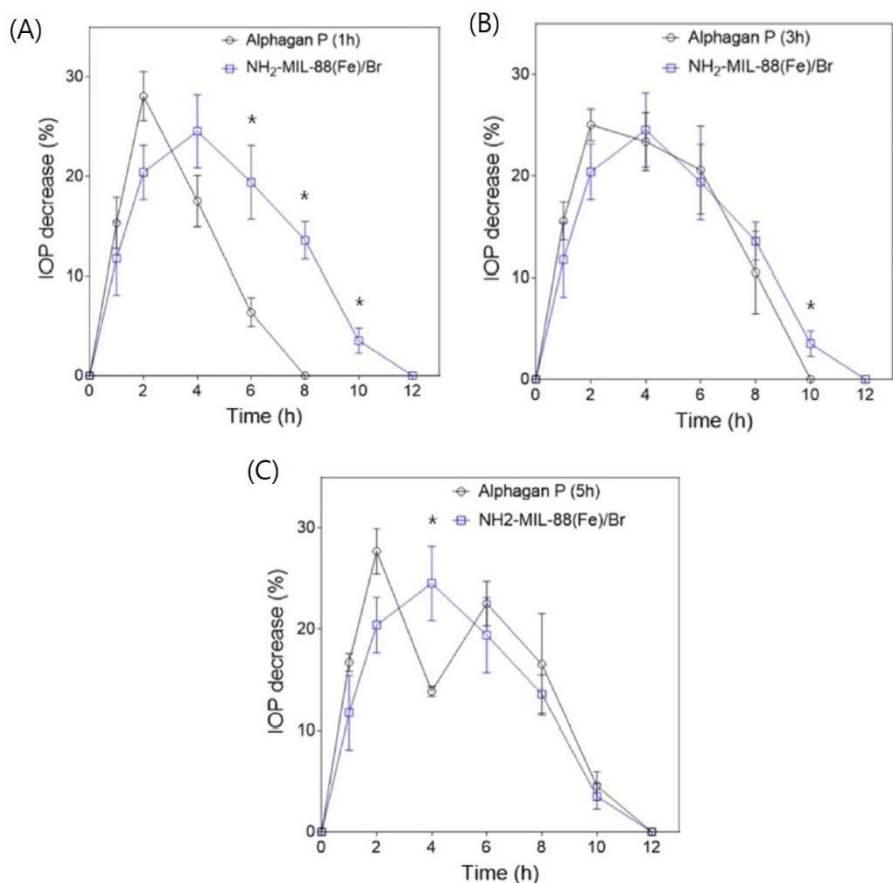
Figure 2.16. Percentage reduction in intraocular pressure (IOP) over time obtained from different Alphagan P administration protocols. The IOP profile was compared with that of $NH_2-MIL-88(Fe)/Br$. Alphagan P was administered at (A) 1 h, (B) 3 h, or (C) 5 h after the first administration. Error bars = $\pm$ SD (n =4).

2.3.6 *In vivo* safety evaluation

In the follow up period of 24 h after a single administration and 7 days after multiple administrations of the $NH_2-MIL-88(Fe)/Br$, the rabbit eyes did not show any apparent complications or eye tissue damages other than mild conjunctivitis. This mild conjunctivitis was not very different from that observed in untreated rabbit eyes, which mostly occur from dehydration of the eye followed by general anesthesia (Figure. 2.17). After multiple administrations of the $NH_2-MIL-88(Fe)/Br$, no systemic exposure of brimonidine was observed.
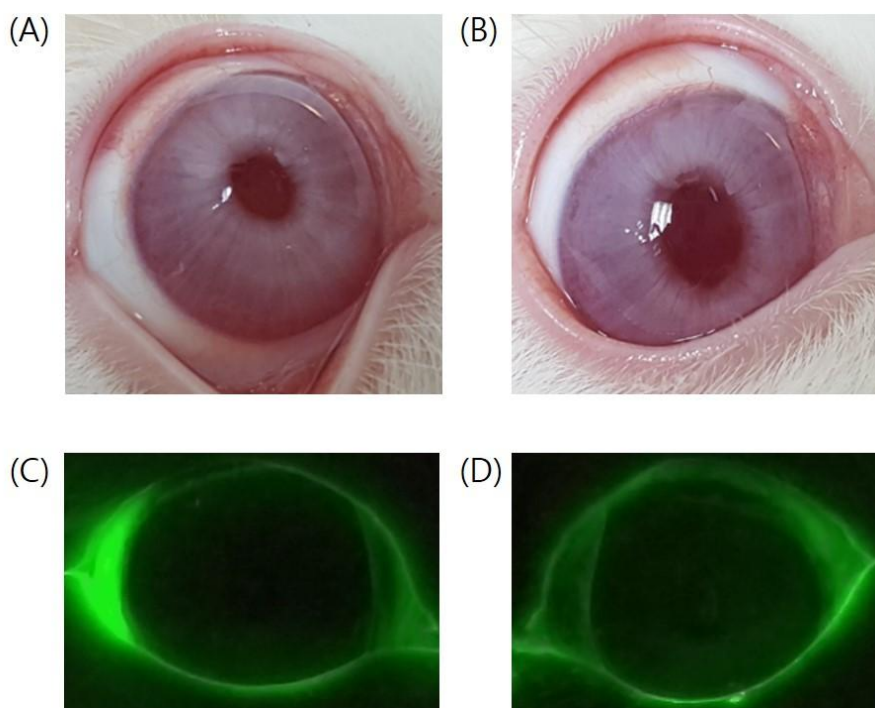
Figure 2.17. Representative images of rabbit eyes for safety evaluation. The optical images of rabbit eyes were obtained (A) before administration and (B) 24 h after a single administration of the $NH_2-MIL-88(Fe)/Br$ suspension. The fluorescent images of fluorescein-stained rabbit eyes were obtained (C) before administration and (D) after 7 days with multiple administrations of the $NH_2-MIL-88(Fe)/Br$ suspension.

2.4 Discussion

MOFs, porous inorganic-organic hybrid materials composed of a biocompatible metal and organic linkers, have attracted much interest as potential drug carriers [13], as the drug molecules can be encapsulated and released in a controlled manner owing to the highly porous structure of the MOFs. Therefore, I conducted the first investigation, to the best of our knowledge, of $NH_2-MIL-88(Fe)$, the MOF microparticles [31], as a potential carrier for topical delivery of an ocular drug, brimonidine, to the eye. Previously, many different particle formulations were suggested as glaucoma drug carriers for topical delivery to the eye.

The $NH_2-MIL-88(Fe)$ particles synthesized in this study have large internal constituent pores and an exceptionally high surface area, which permits an excellent drug-loading capacity. Owing to the molecular size of brimonidine (4.7 x 9.8 Å) [84], the synthesized $NH_2-MIL-88(Fe)$ particles were suitable for encapsulation of brimonidine within its pores (10 Å). In addition, the p–p bond in the benzene structure of brimonidine mutually interacts
with the p–p bond in the ligand 2-aminoterephthalic acid of

$NH_2-MIL-88(Fe)$, which would likely result in more efficient drug loading via physical absorption, as well as sustained drug release from $NH_2-MIL-88(Fe)/Br$ (Figure. 2.7) [85, 86].

In addition, the constituent ligand herein, 2-aminoterephthalic acid, conferred a mucoadhesive property of $NH_2-MIL-88(Fe)/Br$ through the hydrogen bonding and ionic interactions between the $NH_2-MIL-88(Fe)/Br$ and mucin chains [2]. The surface of the $NH_2-MIL-88(Fe)$ is composed of hydrogen-rich organic ligands and amino groups, which can interact with the carboxyl and hydroxyl groups of mucin, respectively, to form a vast number of hydrogen bonds. In addition, the mucin is negatively charged under biological conditions at pH 7 [87], whereas $NH_2-MIL-88(Fe)$ presents NH^{3+} to yield a positive surface charge. Therefore, the ionic interaction can also be attributed to the mucoadhesive properties of $NH_2-MIL-88(Fe)/Br$ prepared in this work [88]. Therefore, this inherited mucoadhesion and exceptionally high specific surface could synergistically result in the long preocular residence time (>4h) observed for $NH_2-MIL-88(Fe)/Br$ in this study (Figure. 2.12).

Owing to the *in vitro* drug release profile (Figure. 2.7)

and the *in vivo* preocular retention properties (Figure. 2.12), prolonged availability of brimonidine was expected in the anterior segment of the eye, leading to a higher bioavailability of brimonidine in the aqueous humor and, therefore, a prolonged duration of IOP-lowering effect in comparison with that reported for the solution form of brimonidine, such as Alphagan P, which was cleared almost immediately after administration (Figures. 2.13 and 2.14). Unlike multiple daily administrations needed for Alphagan P [65], the 12-h period of IOP decrease with the $NH_2-MIL-88(Fe)/Br$ would be advantageous in an aspect of patient medication adherence as the administrations would be needed twice per day simply before and after night sleep.

Generally, additional fluid introduced topically to the eye along with drug-delivery carriers results in expedited tear production, which leads to even faster clearance of the drug-delivery carriers [73, 89]. For this reason, to obtain meaningful enhancement in drug bioavailability, the mucoadhesive microparticles were often formulated in a dry tablet or suspension containing an additive material to increase the tear viscosity, hence further increasing the preocular residence time

of the microparticles [72, 90, 91]. However, such formulations may cause eye discomfort or blurred vision. On the other hand, the delivery of $NH_2-MIL-88(Fe)/Br$ in a suspension formulation along with an external fluid only still exhibited enhanced bioavailability of brimonidine, which implied the strong mucoadhesion synergistically improved by a high specific surface area. For a more prolonged efficacy of ocular drug bioavailability, the drug formulations could be injected into the ocular tissues, such as the conjunctiva or vitreous humor [92-94]; however, this would be invasive, compared with topical drug administration to the eye, mostly favored by the patients [56].

The $NH_2-MIL-88(Fe)$ were made in micron-size (Figure. 2.6) and thus, they would stay at the preocular space to release the drug molecules into tear. On the other hand, the nanoparticles themselves would permeate into the eye tissues due to their small sizes [95-97]. The $NH_2-MIL-88(Fe)$ can be fully degraded in biological fluid in 12 h (Figure. 2.7), giving Fe^{3+} and 2-amino terephthalate, which are known to be generally biocompatible [31, 98]. Therefore, the $NH_2-MIL-88(Fe)$ would not be accumulated in the eye and they are

expected to not cause considerable side effects. In this aspect, the $NH_2-MIL-88$(Fe) would be more advantageous compared with the chitosan microparticles often employed for glaucoma drug delivery because they needed crosslinking to allow for sustained drug release, hence difficulty in biodegradation [99–101]. The *in vitro* cytotoxicity assessment (Figure. 2.9) and *in vivo* safety evaluation (Figure. 2.17) performed in this study confirmed that $NH_2-MIL-88$(Fe) did not induce any apparent cytotoxicity or eye complications. However, as a long-term exposure of Fe^{3+} could be a concern in terms of ocular safety [102], further study is needed in perspectives of clinical applications of the formulations proposed herein.

Because mucus covers many parts of body, such as the eyes,nasal cavity, stomach, and intestines, mucoadhesive drug delivery vehicles have been extensively investigated over the past two decades [103]. They have been designed to form a chemical and/or physical interaction between the carriers and mucous layer to enable long-term mucosal retention at the specific site of interest [104–106]. Thus, the drug loaded in the carrier could be released slowly while the carriers were present longer at the target site in the body, thereby providing

improved drug efficacy [103, 107]. Therefore, the developed mucoadhesive $NH_2-MIL-88(Fe)$ particles may also be applicable to drug delivery for a variety of mucus-lined routes.

2.5 Conclusion

A Fe-based MOF, $NH_2-MIL-88(Fe)$, was successfully synthesized by using a solvothermal method and used for the first time as a carrier for the topical drug delivery of an ocular drug, brimonidine, to the eye. $NH_2-MIL-88(Fe)$ possessed mucoadhesive properties and exhibited the sustained drug release of encapsulated brimonidine. *In vivo* evaluations showed that $NH_2-MIL-88(Fe)/Br$ remained on the preocular surface for a prolonged period, leading to a prolonged duration of IOP reduction and the promotion of the ocular bioavailability of brimonidine. Therefore, $NH_2-MIL-88(Fe)$ represents a promising carrier for topical drug delivery to the eye for the improved absorption of ophthalmic drugs.

Chapter 3

Amine−grafted SBA−15 for ophthalmic delivery of dexamethasone

3.1 Introduction

Mesoporous silica is a material with high porosity and large surface area, because of which it has been extensively tested to variously function as catalysts, adsorbents, molecular sieves, and separation− and sensing agents [108−110]. Moreover, mesoporous silica has recently attracted great interest for possible biomedical application [111−113]. Owing to a tailored mesoporous structure, pore volume, huge surface area, and controllable morphology, as well as selective surface

functionalization, many different types of mesoporous silica particles have been explored for controlled and targeted drug delivery [114-117].

In the field of drug delivery, topical delivery of drugs to the eye poses the problem of low drug bioavailability (< 5%) as conventional eye drops are cleared rapidly from the surface of the eye due to blinking and rapid tear turnover, most of which would be drained via a nasolacrimal duct [118]. To enhance ocular drug bioavailability after topical administration to the eye, it is required that drug carriers remain on the eye surface for a longer time. A variety of micro- and nano-particles have been proposed to resolve this issue, among which the particles composed of mucoadhesive materials have drawn a great deal of interest [2, 119]. Mucoadhesive particles are known to adhere to the mucin present on the eye surface, and thereby, have the potential to improve retention of drugs in the preocular space. The mucoadhesive property of these particles can largely be explained by the formation of ionic complexes and hydrogen bonds between the mucoadhesive material and mucin [12, 120], which could be found with the materials possessing positively charged amine groups, and hydroxyl and carboxyl groups, respectively.

In view of these benefits, I propose the use of amine-grafted SBA-15 mesoporous silica particles (i.e., APS-SBA-15) as carriers for topical drug delivery to the eye. Silica is rich

in hydroxyl groups that can form hydrogen bonds with mucin. The amine groups introduced at the surface of the particles will further improve mucoadhesion by allowing formation of an ionic complex with the negatively charged mucin. Here, I have employed the drug, dexamethasone to be loaded in the mesopores of APS−SBA−15 because it is commonly prescribed for the treatment of various inflammatory eye diseases in clinical settings and is administered as eye drops [121, 122]. I hypothesized that after topical administration to the eye, APS−SBA−15 loaded with dexamethasone will stay longer on the eye surface and release the drug in a sustained manner, hence eventually improving ocular drug bioavailability.

To test this hypothesis, I synthesized SBA−15 particles by the sol−gel method as described previously [123]. Briefly, I used a block copolymer, Pluronic® P123, as micelle−forming surfactant and tetraethyl orthosilicate (TEOS) as a silica precursor. To allow the formation of amine functional groups, the SBA−15 particles were conjugated with aminopropylsilanes via post−synthetic grafting. The resulting APS−SBA−15 possessed mesopores with a cationic charge, and thus, a negatively−charged drug, dexamethasone, could be encapsulated and released in a sustained manner.

I characterized the SBA−15 and APS−SBA−15 prepared here via powder X−ray diffraction (PXRD), N_2 adsorption−desorption analysis, elemental analysis (EA), and

scanning electron microscopy (SEM) to confirm their successful fabrication. I also examined the mucoadhesive property of the drug-loaded SBA-15 and APS-SBA-15 (i.e., DXS@SBA-15 and DXS@APS-SBA-15, respectively) under *in vitro* experimental conditions. To assess *in vivo* efficacy, I applied the drugloaded particles topically to rabbit eyes followed by evaluation of drug concentration in the aqueous humor (AH), which was then compared with that of Maxidex®, which is a clinically-approved form of dexamethasone applied as eye drop.

3.2 Materials and Methods

3.2.1 Materials

Pluronic® P123 (triblock poly(ethylene oxide)$_{20}$ poly(propylene oxide)$_{70}$-poly(ethylene oxide)$_{20}$, M.W. = ~5800), TEOS (assay =98%), and cetyltrimethyl ammonium bromide (CTAB, assay = 99%), (3-aminopropyl) triethoxysilane (APS, assay = 99%), phosphate-buffered saline tablets (0.01M phosphate buffer, pH 7.4), Schiff's fuchsin sulfite reagent, mucin type III (sialic acid = 0.5–1.5%), and periodic and acetic acid were purchased from Merck (Germany). Dexamethasone was obtained from Tokyo Chemical Industry (Japan). Proparacaine hydrochloride

(Alcaine, 0.5% ophthalmic solution), ethanol (assay = 94.5%), and surgical sponge (PVA Spears, Network Medical Products, UK) were supplied by Seoul National University Hospital Biomedical Research Institute (Seoul, Korea), Daejung Chemical (Korea), and Medimaru (Korea), respectively. Xylazine (Rompun), ketamine hydrochloride (Ketamine), and acepromazine maleate (Sedaject) were purchased from BK Pharm (Korea). Maxidex® (0.1% dexamethasone ophthalmic solution) was obtained from Alcon (USA).

3.2.2 Particle preparation

I prepared the SBA-15 particles using the Stöber process (Figures 3.1 and 3.2) according to the previously reported procedure with slight modifications [123]. Pluronic® P123 (4 g) and CTAB (0.2 g) were dissolved in a solution containing 104 mL of deionized water, 20 mL of ethanol, and 20 mL of 2M HCl solution. The resulting mixture was stirred for 30 min at 50 ℃, followed by dropwise addition of 8.4 mg of TEOS with vigorous stirring. The reaction medium was then aged for 5 h at 60 ℃ without stirring. The solid product thus obtained was filtered and washed thoroughly with deionized water and ethanol to

remove any excess surfactants or precursors. Finally, the white particles were filtered and dried at 100 °C for 12 h. Calcination was then performed on this solid product by increasing the temperature from 25 °C to 550 °C at a rate of 1 °C /min and then maintaining it at 550 °C for 5 h in a furnace under N_2 flow. To obtain APS-SBA-15 (Scheme 1(B)), 200 mg of calcined SBA-15 was suspended in 30 mL of toluene, and 2 mL of APS was added to it with stirring. The reaction was carried out in a round bottom flask equipped with a glass condenser to reflux toluene at 110 °C for 3 h. After the reaction was completed, the particles were filtered (PVDF4547A, 0.45 μm pore size, polytetrafluoroethylene membrane filter, HYUNDAI Micro, Korea), washed with toluene and ethanol, and then dried in an oven at 100 °C for 6 h.

To load dexamethasone, the particles were pretreated at 120 °C under vacuum for 3 h to remove moisture. After that, 200 mg of the SBA-15 or APS-SBA-15 particles were immersed in 30 mL of a dexamethasone solution in ethanol (1 mg/mL) for 24 h to yield DXS@SBA-15 or DXS@APS-SBA-15 particles, respectively. The resulting particles were then filtered (PVDF4547A, 0.45 μm pore size,

polytetrafluoroethylene membrane filter, HYUNDAI Micro, Korea), washed three times with copious ethanol, and dried at 90 ℃ for 5 h.
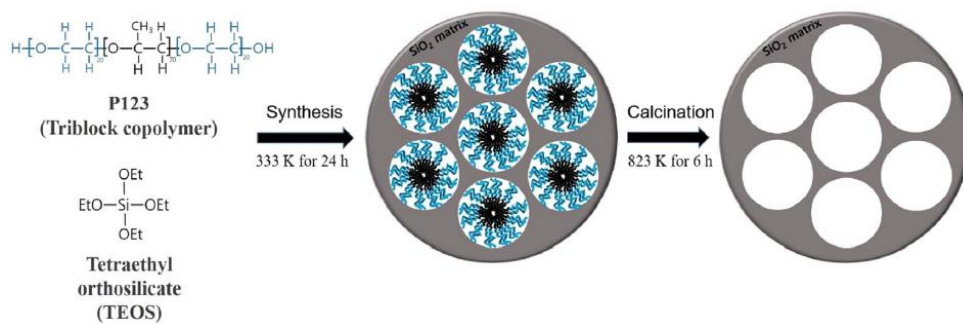
Figure 3.1. Schematic illustration of the synthesis of SBA−15.
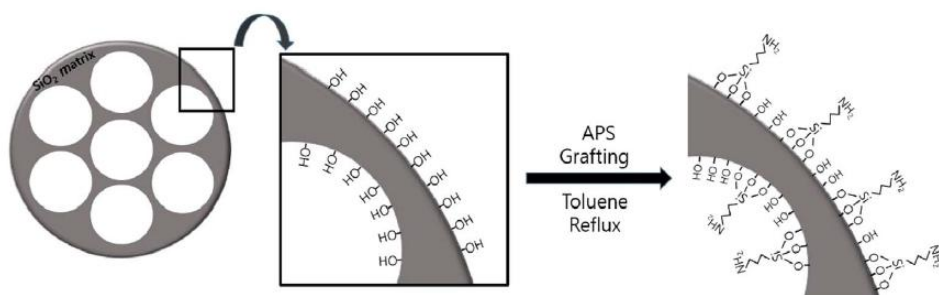
Figure 3.2. Schematic illustration of the synthesis of APS−SBA−15.

3.2.3 Characterization

To assess the crystalline structure, the particles were analyzed via powder X-ray diffractometer (PXRD; SmartLab, Rigaku, Japan) with Cu Kβ radiation at 3 kW over a range of 0.5° < 2θ < 10° (scan speed =0.02°/min). The gas sorption analyzer (Autosorb-iQ 2ST/MP, Quantachrome Instruments, USA) was used to obtain nitrogen isotherms, where the surface area and pore size distribution were obtained by the Brunauer-Emmett-Teller (BET) and Barrett-Joyner-Halenda (BJH) methods, respectively [124]. The particle size distribution was measured by the dynamic light scattering (DLS) method in a particle size analyzer (ELS-2000ZS, Otsuka Electronics, Japan). Briefly, the particles were suspended in deionized water at a concentration of 100 ppb. To measure the amount and distribution of nitrogen in the particles, an elemental analyzer (FlashSmart™ Elemental Analyzer, Thermo Fisher, USA) and transmission electron microscope (JEMF200, JEOL, Japan) were used. The particle morphology was examined using SEM (JSM-7800F Prime, JEOL, Japan). For SEM imaging, the particles were sputter-coated with platinum (Sputter Coater 108 auto, Cressington Scientific Instruments, UK).

To measure the drug loading amount, 5 mg of the DXS@SBA-15 and DXS@APS-SBA-15 were each immersed in 20 mL of a phosphate buffered saline (PBS, pH 7.4, 10 mM) solution. In order to fully extract the drug, the suspension was agitated at 125 rpm in a shaking incubator (SI-600R, Jeio Tech, Korea) at 37 ℃ for 48 h. After that, the suspension was centrifuged at 10,000 rpm for 10 min, and 1 mL of the supernatant was collected and measured using high performance liquid chromatography (HPLC, Agilent 1260 series, Agilent Technologies, USA) with a poroshell column (C18, 2.7 μm-pore, 4.6 ×100 mm, Agilent Technologies, USA) at a 1 mL/min feed rate of the mobile phase [a mixture of acetonitrile and 20mM PBS at pH 2.5 (v/v= 40:60)]. The injection volume of the samples was 10 μL and the UV absorbance was measured at 230 nm. The encapsulation efficiency (%) was calculated from the following equation:

$$\text{Encapsulation efficiency } (\%) = \frac{\text{Drug mass in particles}}{\text{Initially fed drug mass}} X100$$

3.2.4 *In vitro* drug release study

Analysis of drug release was performed on 5 mg of the drug-loaded particles, i.e., DXS@SBA-15 and DXS@APS-SBA-15, in 30 mL of pH7.4 PBS, where a good sink condition of dexamethasone could be maintained. The release medium with the particles was incubated in a shaking incubator (SI-600R; Jeio Tech, Seoul, Korea) at 37 ℃ with continuous stirring at 125 rpm. At predetermined times, a 5 mL of the release medium was collected, and an equal volume of fresh buffer was added back. The sampled release media were assayed by HPLC as described above to measure the amount of dexamethasone released. The experiments were performed in triplicates.

3.2.5 *In vitro* mucoadhesion study

To examine the adsorption of mucin to the particles, 2 mg of the DXS@SBA-15 or DXS@APS-SBA-15 was immersed in 2 mL of an aqueous solution of type III mucin (0.5 mg/mL) for 0.5 h [69]. After the interaction, the particles were collected by centrifugation at 10,000 rpm for 10 min. The collected particles were then re-suspended in deionized water at a concentration of 500 ppb, and their surface charge was assessed using Zetasizer (Nano ZS, Malvern, UK). I also performed

quantitative analysis on mucin adsorption according to a previously reported protocol with modifications [71, 80]. Briefly, an aqueous solution of type III mucin (1 mg/mL) was prepared and pretreated by centrifuging at 10,000 rpm for 10 min. Two mL of the supernatant was collected, and 4 mg of the particles were immersed in it. The resulting suspension was incubated in a shaking incubator (SI-600R;Jeio Tech, Seoul, Korea) at 37 °C for different time periods: 1, 2, 4, and 24 h. After incubation, each suspension was centrifuged at 10,000 rpm for 10 min and 1 mL of the supernatant containing non-adsorbed free mucin was collected. To the collected supernatant, 100 μL of periodic acid diluted with acetic acid was added; the mixture was then incubated in a shaking incubator for 2 h at 37 °C. After that, 100 μL of Schiff's reagent was mixed with the resulting mixture at 25 °C for 30 min and the absorbance was measured with a UV/Vis spectrophotometer (UV-1800 240 V, Shimadzu, Japan) at 560 nm. The amount of mucin adsorbed to the particles was calculated by subtracting the measured amount of non-absorbed free mucin from the total amount of mucin in the initial solution (1 mg/mL).

3.2.6 Cytotoxicity test

Cytotoxicity of DXS@APS-SBA-15 and DXS@SBA-15 was evaluated on human primary corneal epithelial cells (HCECs;

PCS-700-010, ATCC, USA) and L929 mouse fibroblast cells (KCLB, Korea) using a cell viability assay kit (EZ-Cytox; Daeillab Service, Seoul, Korea). The HCECs were cultured in a basal medium for corneal epithelial cell (PCS-700-030, ATCC, USA) using a corneal epithelial cell growth kit (PCS-700-040, ATCC, USA) at 37 °C in a humidified 5% CO_2 atmosphere. The L929 cells were cultured in an RPMI 1640 medium containing 10% fetal bovine serum (Gibco, CA, USA) and 1% antibiotic supplement (Penicillin-Streptomycin 10,000 unit/mL, Thermo Fisher Scientific, MA, USA) at 37 °C in a humidified 5% CO_2 atmosphere.

To test cytotoxicity, 100 μL of the cell suspension (5.0 × 10^4 cells/mL) was seeded on each well of a 96-well plate. After 24 h, DXS@APSSBA-15 or DXS@SBA-15 were added to each well at varying concentrations: particle concentrations of 0.02, 0.05, 0.1, 0.2, 0.5, and 1 mg/mL were introduced with both HCEC and L929 cells. The plate was then incubated at 37 °C for 24 h in a 5% CO_2 humidified atmosphere (N = 8). To assess cell viability, 10 μL of an EZ-Cytox solution was added to each well, and the plates were incubated for another hour at 37 °C. The plate was then read at 450 and 600 nm using a microplate reader (SpectraMax 190 Microplate Reader; Molecular Devices, USA). Cell viability was calculated using the following equation: Cell viability (%) = (absorbance at 450 nm of the well with the particles – absorbance at 600 nm of the

well with the particles)/(absorbance at 450 nm of the well without treatment − absorbance at 600 nm of the well without treatment) × 100.

3.2.7 Animal experiments

For *in vivo* efficacy evaluation, I employed eyes of healthy, male New Zealand White rabbits (1.8–2.5 kg, Orient Bio, Korea). The experimental protocol using in this study was approved by the Institutional Animal Care and Use Committee at the Biomedical Research Institute of the Seoul National University Hospital (IACUC No. 16–0085).

I administered a 35 μL suspension of DXS@APS−SBA−15 or DXS@SBA−15 with an equivalent dose of 35 μg of dexamethasone topically to rabbit eyes, respectively. As per the amount of drug loaded in the particles, the particle concentrations in the suspension were 14.65 and 34.11 mg/mL for DXS@APS−SBA−15 and DXS@SBA−15, respectively. For comparison, a 35 μL drop of Maxidex® with the same dose was also applied. At scheduled times after administration, I measured the drug concentrations in the AH. For this, rabbits were anesthetized with a subcutaneous injection of a cocktail of 17.5 mg/kg ketamine, 5 mg/kg xylazine, and 0.2 mg/kg acepromazine, and approximately 100 μL of AH was then aspirated using a 31 G syringe (Jung Rim Medical, Korea). Five

eyes (i.e., one eye for each animal) were tested for each type of formulation applied at each scheduled time and subjected to statistical analyses. The concentration of dexamethasone in the collected samples was determined by an HPLC-mass spectrometer (LC-MS, Agilent 6120 Series Quadrupole LC/MS, Agilent Technologies, USA) using an EC-C18 Poroshell column (4.6 × 50 mm, 2.7 μm pore size, Agilent Technologies, USA). The mobile phase was composed of 0.1% formic acid and acetonitrile (50:50, v/v). The flow rate and sample injection volumes were 0.5 mL/min and 10 μL, respectively. The column temperature was maintained at 30 °C and the retention time was 6.77 min (detection mass ion = 393).

3.2.8 Statistical analyses

Mann-Whitney U-test was used to perform statistical analyses on the extent of mucin adsorption to the particles and drug concentrations observed in the AH, where $p < 0.05$ was considered statistically significant (SPSS version 22, IBM, USA). For mucin adsorption analysis, the amount of DXS@SBA-15 and DXS@APS-SBA-15 at each sampling event after incubation with mucin was compared. For analysis of drug concentrations in AH, values with the particles, DXS@SBA-15 and DXS@APS-SBA-15, as well as only Maxidex® at each sampling event after administration were

compared.

3.3 Results

3.3.1 Particle characterization

I first assessed the physical properties of the SBA-15 particles prepared here following a previously described protocol [123]. The PXRD patterns of SBA-15 both before and after calcination and the PXRD patterns of APS-SBA-15 displayed a well-resolved pattern with a single broad peak in the 2θ range of 0.5–1° as previously reported (Figure. 3.3) [125]. This result suggested that the mesoporous structure in both types of particles was maintained well after calcination and amine-grafting procedures. According to the N_2 adsorption-desorption isotherm (Figure. 3.4), both SBA-15 and APS-SBA-15 exhibited a distinct pattern of the Type IV isotherm, which further confirmed the presence of mesopores in the particles. The BET and BJH analyses revealed that the specific surface area, average pore diameter, and total pore volume of SBA-15 were 658.79m^2/g, 7.18 nm, and 1.15 cm^3/g, respectively (Figure. 3.4), which appeared to decrease slightly to 527.14m^2/g, 5.32 nm, and 0.74 cm^3/g, respectively, after amine-grafting (i.e., APS-SBA-15) (Figure. 3.5). The incorporated nitrogen content in the APS-SBA-15 was

measured to be 2.01 wt% according to elemental analysis; this indicated the presence of 1.43 mmol amine groups per g of APS−SBA−15. The TEM−EDS map revealed a homogenous distribution of amine groups in APS−SBA−15, while no peaks of nitrogen were observed in SBA−15 (Figures. 3.6 and 3.7). All particles prepared here (i.e., the SBA−15, APS−SBA−15, DXS@SBA−15, and DXS@APS−SBA−15) exhibited a spherical shape with a diameter of about 2–4 μm as shown in Figure. 3.8. Due to the particle size being much smaller than 10 μm, the particles prepared here were not expected to cause eye irritation (Figures 3.9 and 3.10) [126].
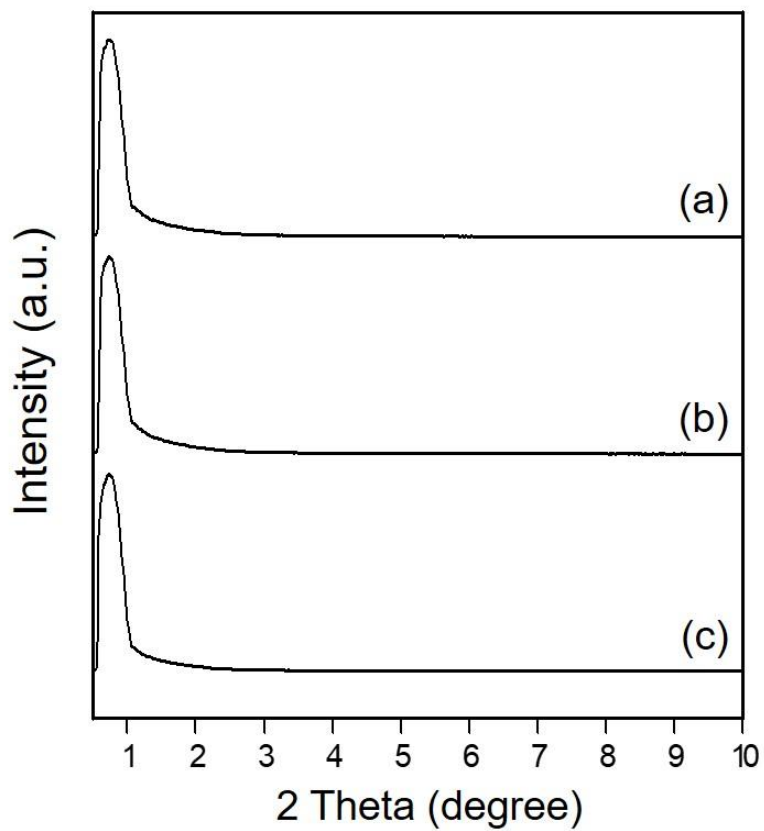
Figure 3.3. Powder X-ray diffraction patterns of (a) SBA-15 before calcination, (b) SBA-15 after calcination, and (c) APS-SBA-15.
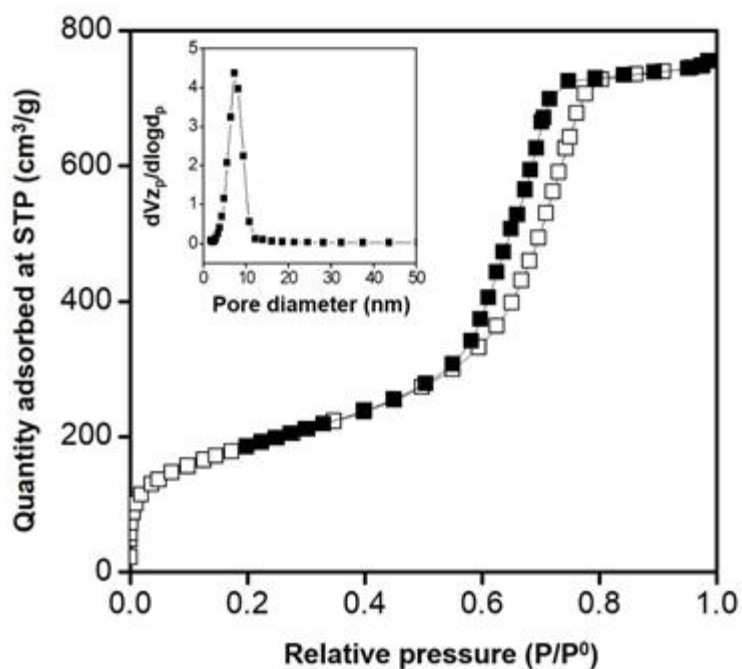
Figure 3.4. N$_2$ adsorption−desorption isotherm profiles and pore size distribution curves (in the insets) for SBA−15 (■− adsorption, □−desorption).
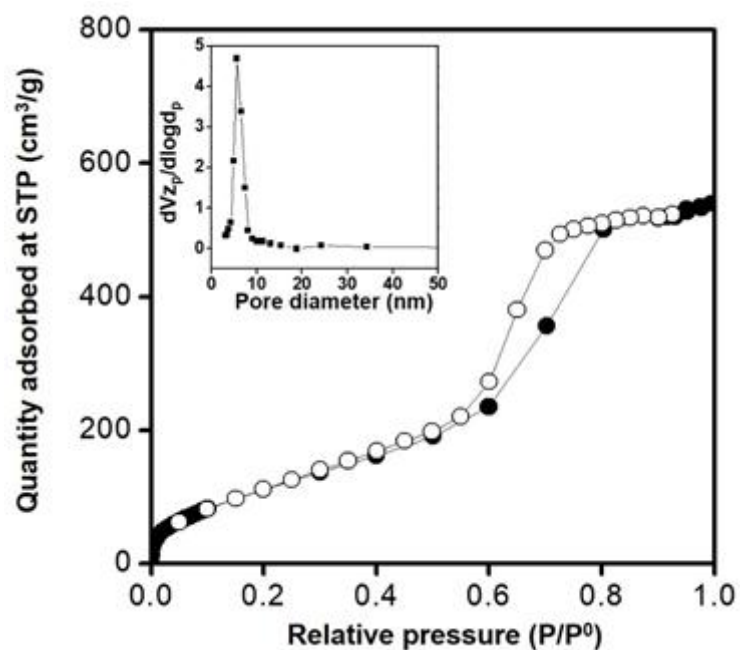
Figure 3.5. N$_2$ adsorption−desorption isotherm profiles and pore size distribution curves (in the insets) for APS−SBA−15 (■−adsorption, □−desorption).
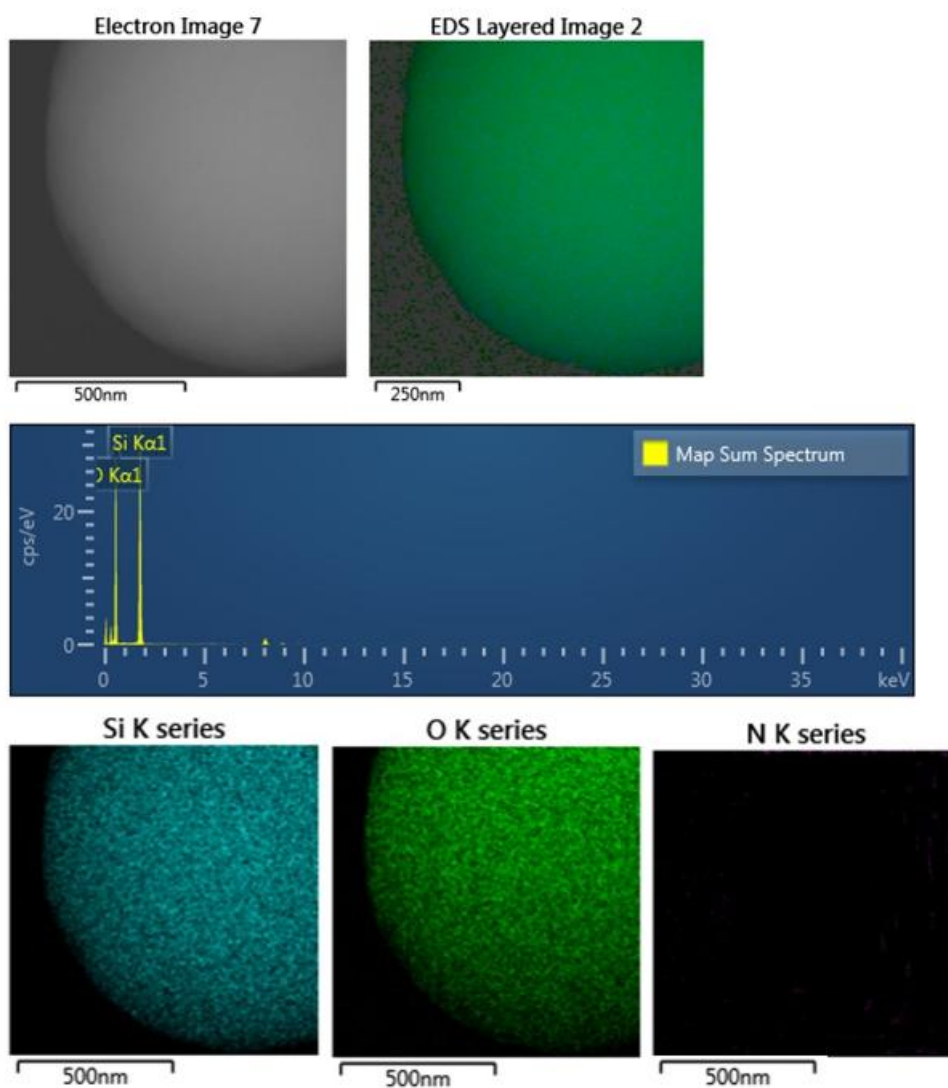
Figure 3.6. TEM−EDS map images of SBA−15.
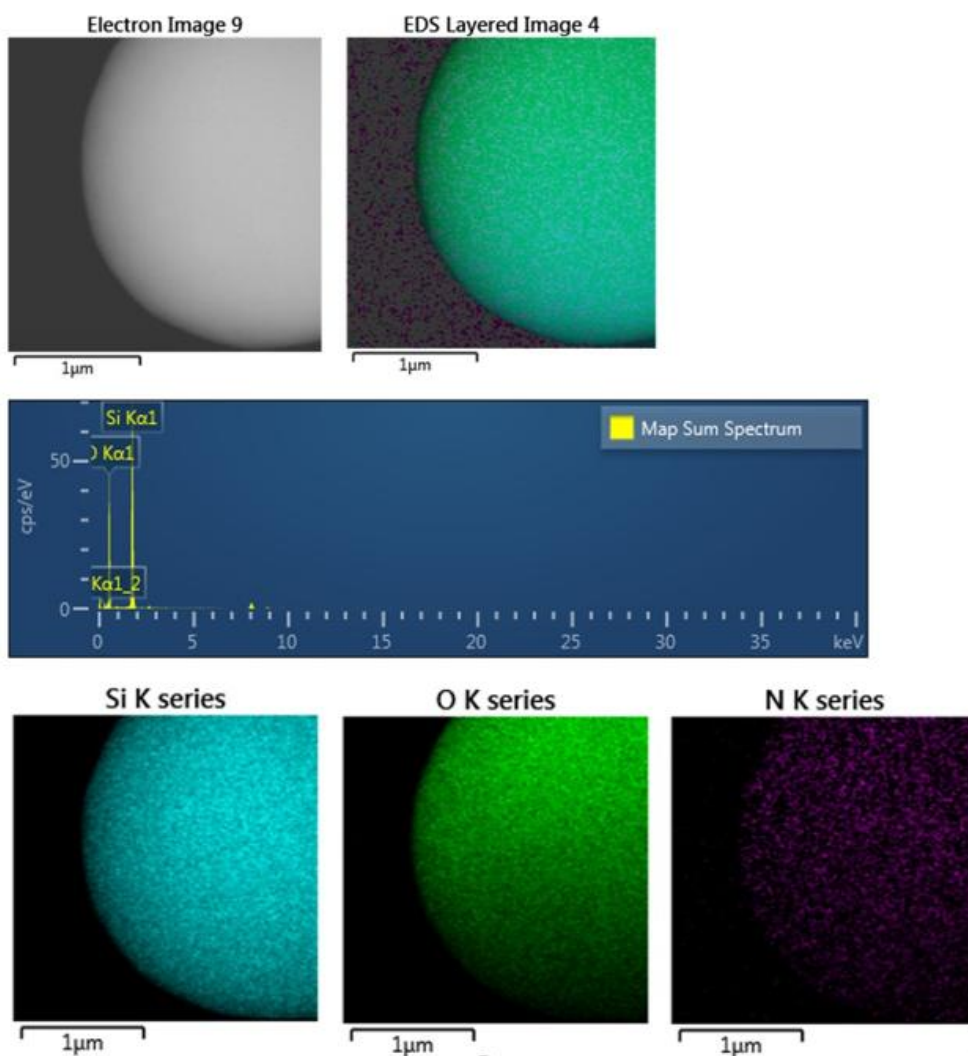
Figure 3.7. TEM−EDS map images of APS−SBA−15. The nitrogen map shows a homogenous distribution of the amine groups in the APS−SBA−15.
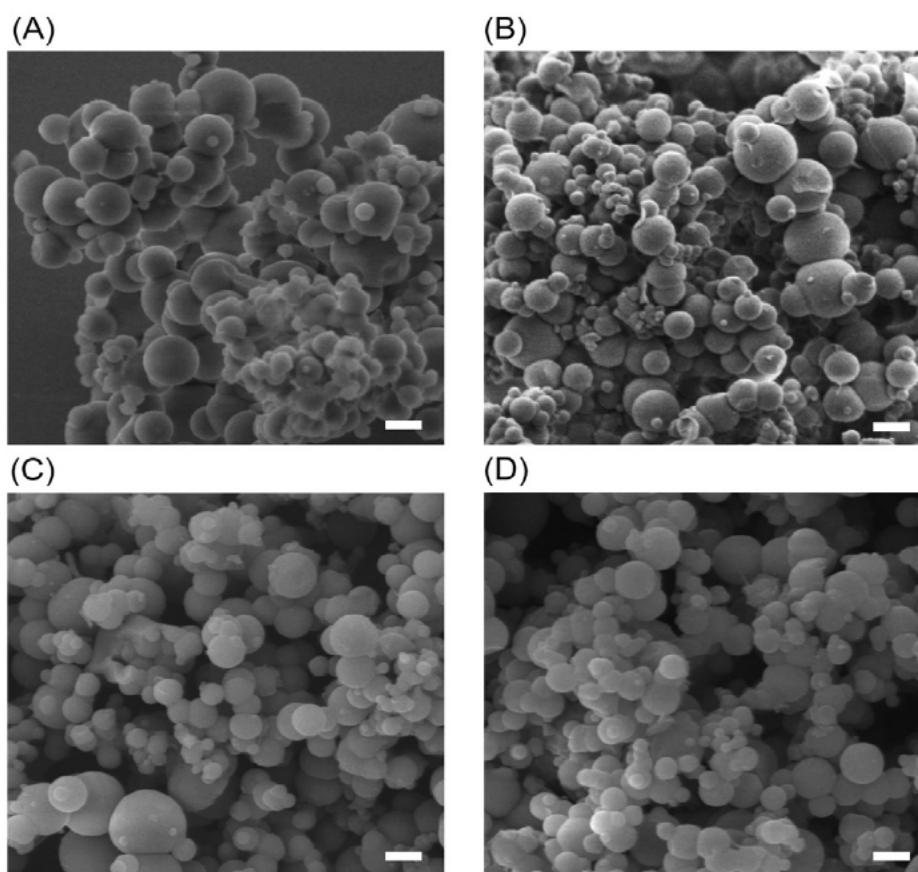
Figure 3.8. Scanning electron microscopy (SEM) images of (A) SBA−15, (B) APS−SBA−15, (C) DXS@SBA−15, and (D) DXS@APS−SBA−15. Scale bars = 1 μm.
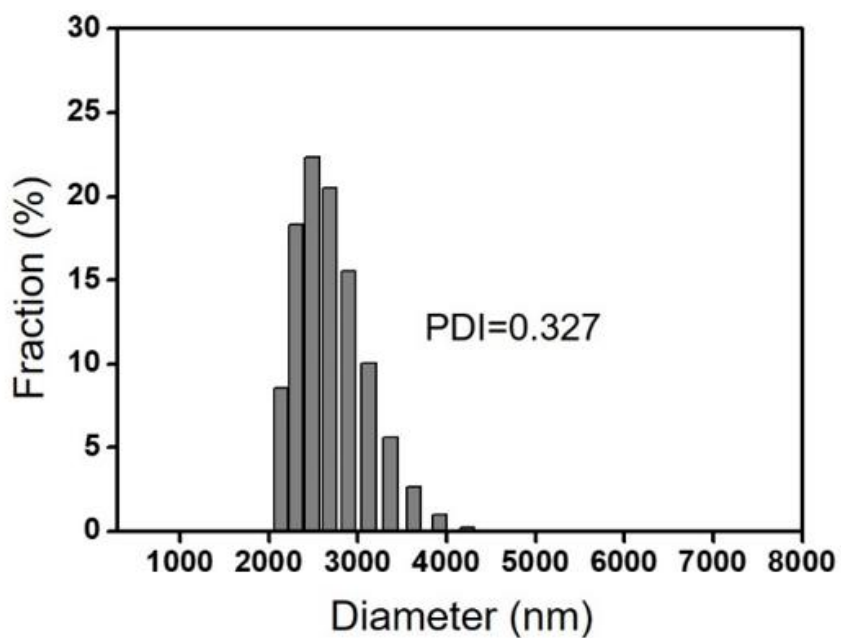
Figure 3.9. Particle size distribution of SBA−15 measured by the dynamic light scattering (DLS) method. The particles were suspended in deionized water at a concentration of 100 ppb.
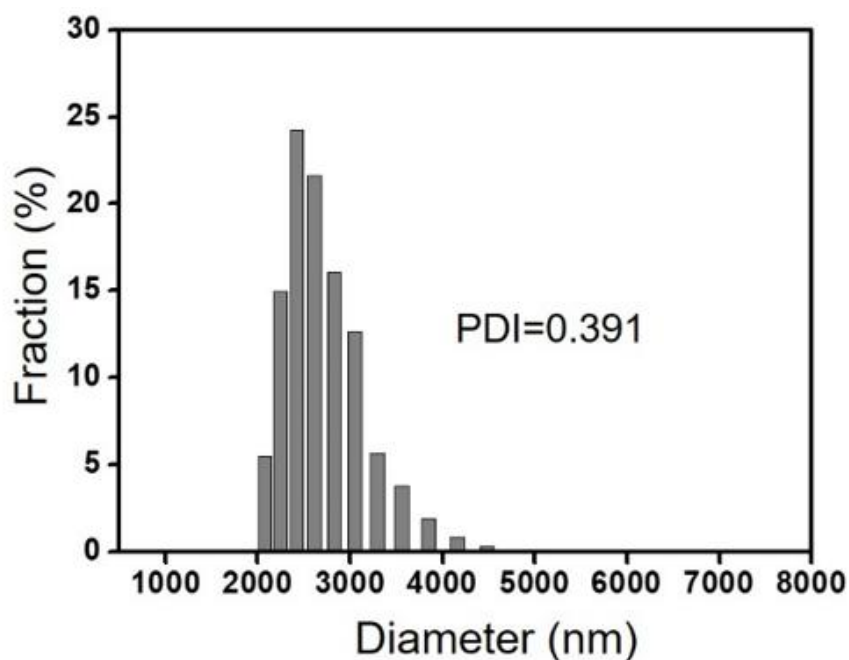
Figure 3.10. Particle size distribution of APS−SBA−15 measured by the dynamic light scattering (DLS) method. The particles were suspended in deionized water at a concentration of 100 ppb.

3.3.2 *In vitro* evaluation

The amounts of drugs loaded in DXS@APS-SBA-15 and DXS@SBA-15 were measured to be 68.23 and 29.31 µg/mg, respectively, with encapsulation efficiencies of 45.4% and 19.5%, respectively, under the drug loading conditions applied in this work. Considering the pore sizes of SBA-15 and APS-SBA-15 (7.18 and 5.32 nm, respectively), the molecules of dexamethasone would be small enough (approximately 8.3 × 15.2 Å) to be loaded in the mesopores of the particles [84]. A higher drug encapsulation efficiency for APS-SBA-15 particles can be attributed to the cationic surface harboring amine groups, which can adhere better with the anionic drug, dexamethasone. According to the *in vitro* drug release analysis (Figure. 3.11), while DXS@SBA-15 released 100% dexamethasone during the first hour, DXS@APS-SBA-15 released the drug in a more sustained manner for 12 h after a 58% burst release during the first hour. For the *in vitro* drug release study, a relatively large volume of PBS was used to maintain a good sink condition (aqueous solubility of dexamethasone = 0.16 mg/mL). Therefore, considering the small volume of tear fluid (~ 10 µL) [78], drug release is expected to be slower, when actually applied to the eye *in vivo*. When tested for safety on L929 cells and HCECs, both DXS@SBA-15 and DXS@APS-SBA-15 appeared to be non-cytotoxic as shown in Figure. 3.12.

To evaluate the surface properties, I measured the change in surface charge of SBA-15 before and after amine functionalization and drug loading. As shown in Table. 3.1, SBA-15 had a negative zeta-potential of -51.3. The negative surface charge of SBA-15 was attributable to the presence of many hydroxyl groups. After APS grafting, APS-SBA-15 had a positive zeta-potential, 26.7 mV, owing to the presence of amino groups. After the loading of an anionic drug, dexamethasone, the zeta potentials were shifted to be - 45.2 and 12.1 mV for DXS@SBA-15 and DXS@APS-SBA-15, respectively.

I also assessed the mucoadhesive property of DXS@SBA-15 and DXS@APS-SBA-15 under *in vitro* environment. For this, I measured the zeta potential of the particles after interaction with mucin. As shown in Table 3.1, after interaction with mucin, the zeta potentials shifted to values closer to that on mucin (-18.6 mV) and were measured to be - 22.1 and - 10.9 mV for DXS@SBA-15 and DXS@APS-SBA-15, respectively. This result implied the presence of adsorbed mucin on the surface of both DXS@SBA-15 and DXS@APS-SBA-15.

According to quantitative measurements (Figure. 3.13), the amount of mucin adsorbed on DXS@SBA-15 was 372 ± 31 µg/mg after 0.5 h of interaction, which increased to 398 ± 37 µg/mg after an hour. Notably, more mucin appeared to be

adsorbed on DXS@APS−SBA−15 with the adsorbed amounts being 561 ± 52 and 589 ± 59 μg/mg after 0.5 and 1 h of interaction, respectively. The mucoadhesive properties of both DXS@SBA−15 and DXS@APS−SBA−15 can be attributed to the presence of abundant hydroxyl groups that form hydrogen bonds with mucin [127]. This phenomenon was more prominent with DXS@APS−SBA−15 as the positively charged amine groups could form ionic complexes with the negatively charged mucin [128].
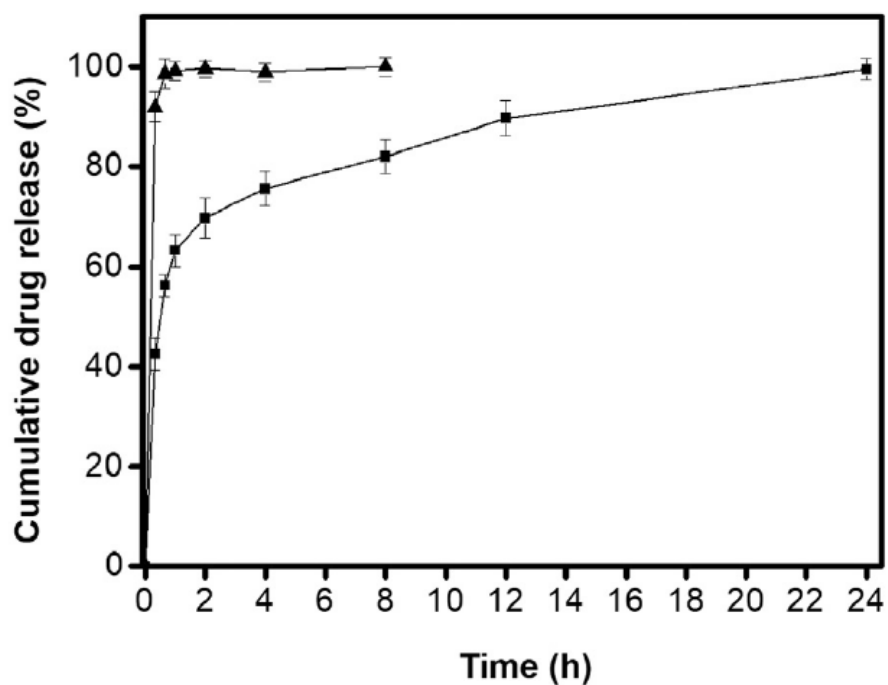
Figure 3.11. *In vitro* release profiles of dexamethasone from (A) DXS@SBA−15 and (B) DXS@APS−SBA−15 in PBS (pH 7.4) at 37 ℃. Error bars = ± SD (n =3).
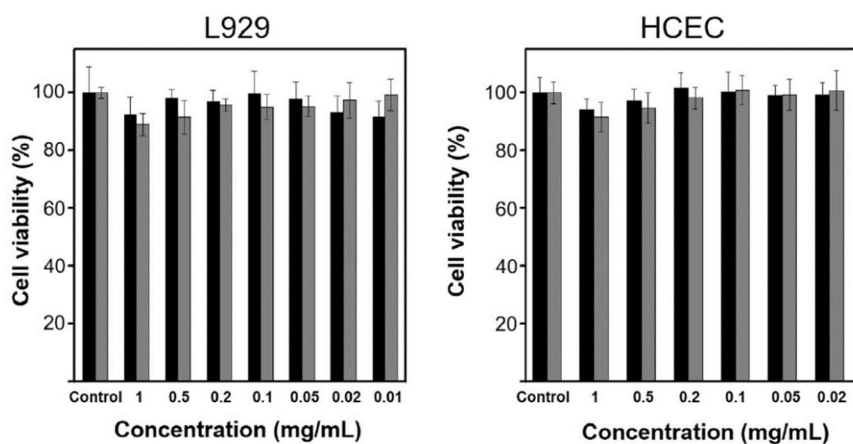
Figure 3.12. *In vitro* cytotoxicity of DXS@SBA−15 (black) and DXS@APS−SBA−15 (grey) assessed on L929 and human primary corneal epithelial cells. Error bars = ± SD (n =8).

Table 3.1. Zeta potential values of mucin, SBA−15, APS−SBA−15 and obtained before/after incubation of DXS@SBA−15 and DXS@APS−SBA−15 with mucin

Samples	Zeta potential (mV)
Mucin	−18.6
SBA−15	−51.3
APS−SBA−15	26.7
DXS@SBA−15	−45.2
DXS@APS−SBA−15	12.1
DXS@SBA−15 with mucin	−22.1
DXS@APS−SBA−15 with Mucin	−10.9
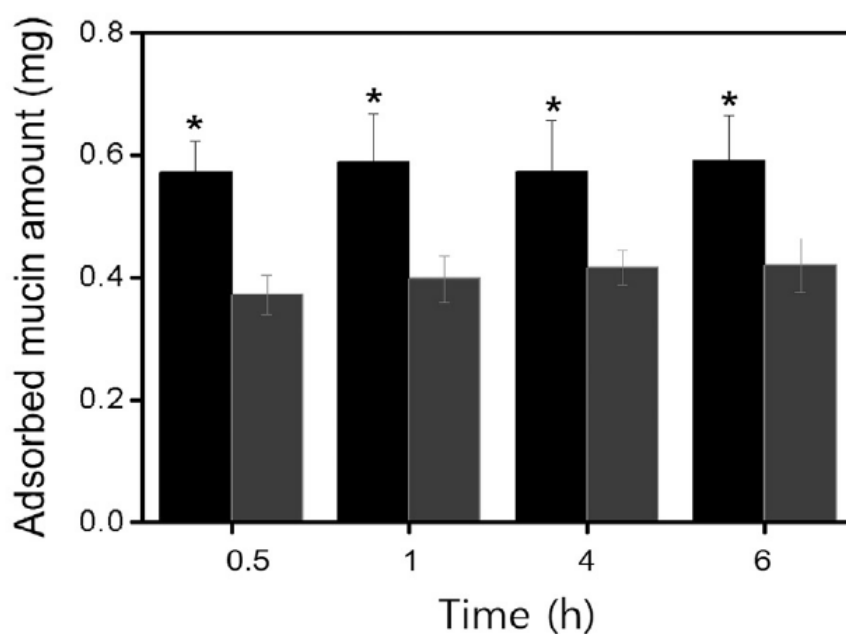
Figure 3.13. Amounts of mucin adsorbed on DXS@APS−SBA−15 (black) and DXS@SBA−15(grey). *At all times of mucin interaction, DXS@APS−SBA−15 was significantly different from DXS@SBA−15. Error bars = ± SD (n =4).

3.3.3 *In vivo* evaluation

To examine *in vivo* efficacy, a suspension of DXS@APS−SBA−15, or DXS@ SBA−15, or a drop of Maxidex® eye drops, was applied topically to rabbit eyes with all three having the same dose of dexamethasone; drug concentrations in the AH were then measured at scheduled times after administration. As shown in Fig. 3.14, drug concentration profiles in the AH were not very different between the rabbits administered DXS@SBA−15 or Maxidex®. Although the DXS@SBA−15 would be mucoadhesive to allow prolonged retention in the preocular space, all the drug was released almost instantaneously from the particles, hence its pharmacokinetic profile was similar to that of the Maxidex® eye drops. On the other hand, the improved ocular bioavailability of dexamethasone was apparent in the form of DXS@APS−SBA−15. Drug concentration in the AH was higher than that with Maxidex® or DXS@SBA−15 after 1–6 h, and the difference was statistically significant ($p < 0.05$). Therefore, the area representing drug concentration under the AH−time curve (AUC) for DXS@APS−SBA−15 (0.92 µg h/mL) was more than 1.8−fold larger than those for Maxidex® (0.49 µg h/mL) and DXS@SBA−15 (0.36 µg h/mL), suggesting a higher amount of drug absorbed into the AH with the DXS@APS−SBA−15.

The mucoadhesive property could be more pronounced in case of APS−SBA−15 due to the presence of amine and

hydroxyl groups (Figures. 3.13 and 3.14). The mesopores could serve as drug reservoirs, while the presence of amine groups in APS−SBA−15 may allow sustained release of negatively−charged dexamethasone (Figure. 3.11). Therefore, when DXS@APS−SBA−15 is topically administered to the eye, it may adhere to the mucous layer in the eye surface, and hence ensure prolonged preocular retention as compared with conventional eye drops that are known to be rapidly cleared from the eye surface [58]. In addition to its longer stay on the eye surface, the drug would be slowly released into the tears to maintain an effective concentration gradient from tear to the AH for a longer time; in this manner, a prolonged adsorption of dexamethasone on the ocular tissues will eventually improve drug bioavailability. The silica particles tested here have already been shown to be biocompatible to a large extent in previous studies, including for their possible applications on the eye [129, 130]. In this study, the APS−SBA−15 did not exhibit cytotoxicity (Figure. 3.12), and there was no eye abnormality after topical administration *in vivo* either.
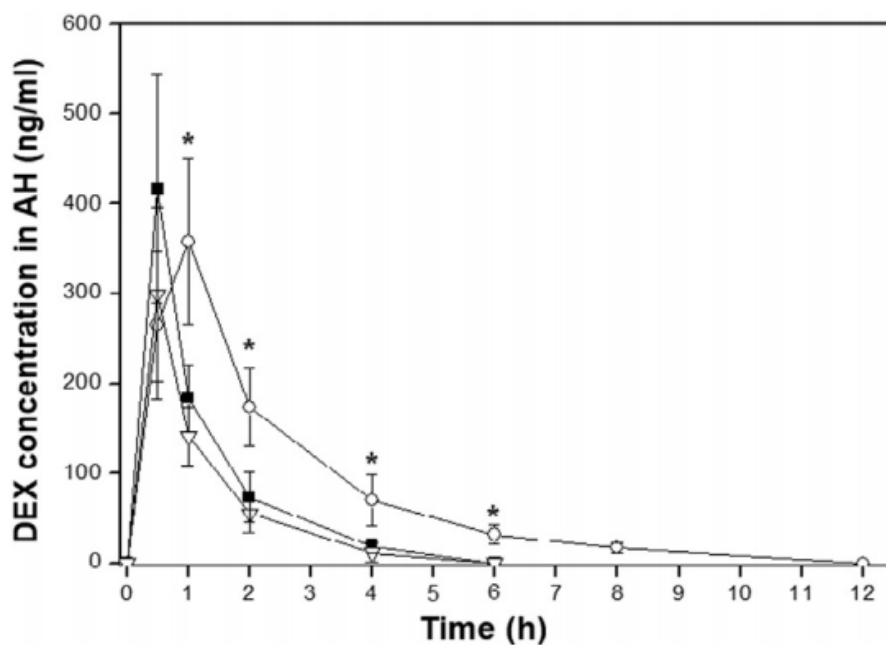
Figure 3.14. Drug concentrations in aqueous humor of rabbit eyes after topical administration of DXS@SBA−15 (■), DXS@APS−SBA−15 (○), and Maxidex® (▽). *At 1, 2, 4, and 6 h DXS@APS−SBA−15 showed a statistically significant difference from DXS@SBA−15 and Maxidex®. Error bars = ± SD (n =5).

4.4 Conclusion

Based on our results, we suggest the use of amine-grafted mesoporous silica particles, i.e., APS-SBA-15, as potential carriers of dexamethasone for topical delivery to the eye. The APS-SBA-15 tested here can be loaded with dexamethasone, which can then be released in a sustained manner because of the interaction of charges on the amine groups on APS-SBA-15 and the negatively charged dexamethasone. The APS-SBA-15 can better adhere to the mucin in the eye, and thus, ensure a prolonged preocular retention. Therefore, when topically administered to the eye *in vivo*, the APS-SBA-15 was observed to stay longer on the eye surface, while releasing the drug slowly, which led to improved ocular bioavailability of dexamethasone. Therefore, we conclude that the amine grafted SBA-15 particles are promising carriers for enhanced bioavailability of topically-delivered ocular drugs.

Chapter 4

Conclusion and Perspective

Effective drug delivery to targeted ocular tissues is essential for the treatment of eye disease. Currently, many researchers are working hard to improve the *in vivo* performance of conventional and novel formulations using state of the art technology. However, in the clinical area, because of the ease of administration and patient compliance, the majority of prescription drugs are administered as eye drops (90%), but still have the problem of low drug bioavailability. To address this problem, I synthesized two highly porous hybrid particles, functionalized their surfaces and evaluated their mucoadhesiveness and drug delivery performance by applying them to ophthalmic drug delivery systems.

In chapter 2. I prepared an iron based metal organic framework, $NH_2-MIL-88(Fe)$, and used the framework for the first time as a carrier for the topical drug delivery of an ocular drug, brimonidine. $NH_2-MIL-88(Fe)$ possesses mucoadhesive properties and exhibited the sustained drug release of encapsulated brimonidine. *In vivo* evaluations showed that $NH_2-MIL-88(Fe)/Br$ remained on the preocular surface for a prolonged period, leading to a prolonged duration of IOP reduction and promotion of the ocular bioavailability of brimonidine. In particular, $NH_2-MIL-88(Fe)/Br$ was naturally degraded in 24 h and disappeared upon administration to the eye. The safety was confirmed in *in vitro* cytotoxicity tests and in vivo experiments.

In Chapter 3, I suggested the use of amine-grafted mesoporous silica particles, (i.e., APS-SBA-15), as potential carriers of dexamethasone for topical delivery to the eye. The APS-SBA-15 tested here was loaded with dexamethasone, which was released in a sustained manner because of the interaction of charges on the amine groups on APS-SBA-15 and the negatively charged dexamethasone. The APS-SBA-15 was evaluated for mucoadhesiveness. In *in vivo* experiments, it adhered to the mucin in the eye, ensuring prolonged preocular retention. Additionally, the safety of the materials for the eye was confirmed in *in vitro* cytotoxicity tests and in vivo experiments for the first time using primary corneal epithelial

cells and rabbit model, respectively. When topically administered to the eye *in vivo*, APS−SBA−15 was observed to stay longer on the eye surface, while releasing the drug slowly, which led to improved ocular bioavailability of dexamethasone.

According to the obtained results, surface amine groups are very effective at enhancing the mucoadhesive properties of the carrier. Due to their mucoadhesiveness, the particles developed in this study were able to stay in the anterior part of the rabbit eye for a long time and helped improve the absorption of the drug. I conclude that iron−based MOFs, such as NH_2−MIL−88(Fe), and amine grafted SBA−15 particles are promising carriers for enhanced bioavailability of topically− delivered ocular drugs.

Over the past several decades, a variety of drug delivery systems using nanotechnology and mucoadhesive polymers have been developed for ophthalmic drug delivery, but are unsuitable for product development. However, the two inorganic material−based porous particles proposed in this study are very promising for drug delivery systems with mucoadhesive properties, because they have excellent performance and are suitable for mass production processes. Therefore, I hope that the results of this study contribute to the development of improved drug delivery systems using mucosa distributed in various parts of the human body (e.g., eyes, nose, hepatobiliary system, small intestine, reproductive tract).

References

[1] A. Foster, S. Resnikoff, The impact of Vision 2020 on global blindness, Eye 19(10) (2005) 1133.

[2] A. Ludwig, The use of mucoadhesive polymers in ocular drug delivery, Advanced drug delivery reviews 57(11) (2005) 1595-1639.

[3] T.R.R.S. Rahamatullah Shaikh, M.J. Garland, A.D. Woolfson, R.F. Donnelly, Mucoadhesive drug delivery systems, Journal of Pharmacy and Bioallied Sciences 3(1) (2011) 89.

[4] N. Salamat-Miller, M. Chittchang, T.P. Johnston, The use of mucoadhesive polymers in buccal drug delivery, Advanced drug delivery reviews 57(11) (2005) 1666-1691.

[5] R. Birudaraj, R. Mahalingam, X. Li, B.R. Jasti, Advances in buccal drug delivery, Critical Reviews™ in Therapeutic Drug Carrier Systems 22(3) (2005).

[6] M.I. Ugwoke, R.U. Agu, N. Verbeke, R. Kinget, Nasal mucoadhesive drug delivery: background, applications, trends and future perspectives, Advanced drug delivery reviews 57(11) (2005) 1640-1665.

[7] N.A. Peppas, J.J. Sahlin, Hydrogels as mucoadhesive and bioadhesive materials: a review, Biomaterials 17(16) (1996) 1553-1561.

[8] R. Birudaraj, R. Mahalingam, X. Li, B. Jasti, Crit. Rev. Ther. Drug Carrier Syst., 3 (22), 295-330, (2005).

[9] N. Peppas, TUFTAD Haberler (Special Issue), 4-8 (2005), Google Scholar.

[10] J.W. Lee, J.H. Park, J.R. Robinson, Bioadhesive□based dosage forms: The next generation, Journal of pharmaceutical sciences 89(7) (2000) 850-866.

[11] J.K. Vasir, K. Tambwekar, S. Garg, Bioadhesive microspheres as a controlled drug delivery system, International journal of pharmaceutics 255(1-2) (2003) 13-32.

[12] J.D. Smart, The basics and underlying mechanisms of mucoadhesion, Advanced drug delivery reviews 57(11) (2005) 1556-1568.

[13] P. Horcajada, T. Chalati, C. Serre, B. Gillet, C. Sebrie, T. Baati, J.F. Eubank, D. Heurtaux, P. Clayette, C. Kreuz, Porous metal-organic-framework nanoscale carriers as a potential platform for drug delivery and imaging, Nature materials 9(2) (2010) 172.

[14] H. Li, M. Eddaoudi, M. O'Keeffe, O.M. Yaghi, Design and synthesis of an exceptionally stable and highly porous metal-organic framework, nature 402(6759) (1999) 276.

[15] D.J. Tranchemontagne, J.L. Mendoza-Cortés, M. O'Keeffe, O.M. Yaghi, Secondary building units, nets and bonding in the chemistry of metal-organic frameworks, Chemical Society Reviews 38(5) (2009) 1257-1283.

[16] S. Couck, J.F. Denayer, G.V. Baron, T. Rémy, J. Gascon, F. Kapteijn, An amine-functionalized MIL-53 metal- organic framework with large separation power for CO2 and CH4, Journal of the American Chemical Society 131(18) (2009) 6326-6327.

[17] S.M. Cohen, Postsynthetic methods for the functionalization of metal-organic frameworks, Chemical reviews 112(2) (2011) 970-1000.

[18] D. Farrusseng, Metal-organic frameworks: applications from catalysis to gas storage, John Wiley & Sons2011.

[19] A.R. Millward, O.M. Yaghi, Metal- organic frameworks with exceptionally high capacity for storage of carbon dioxide at room temperature, Journal of the American Chemical Society 127(51) (2005) 17998-17999.

[20] J. Della Rocca, D. Liu, W. Lin, Nanoscale metal-organic frameworks for biomedical imaging and drug delivery, Accounts of chemical research 44(10) (2011) 957-968.

[21] A.C. McKinlay, B. Xiao, D.S. Wragg, P.S. Wheatley, I.L. Megson, R.E. Morris, Exceptional behavior over the whole adsorption- storage- delivery cycle for NO in porous metal organic frameworks, Journal of the American Chemical Society 130(31) (2008) 10440-10444.

[22] K.M. Taylor-Pashow, J. Della Rocca, Z. Xie, S. Tran, W. Lin, Postsynthetic modifications of iron-carboxylate nanoscale metal- organic frameworks for imaging and drug delivery, Journal of the American Chemical Society 131(40) (2009) 14261-14263.

[23] J.L. Rowsell, O.M. Yaghi, Metal-organic frameworks: a new class of porous materials, Microporous and mesoporous materials 73(1-2) (2004) 3-14.

[24] M.X. Wu, Y.W. Yang, Metal-Organic Framework (MOF)☐Based Drug/Cargo Delivery and Cancer Therapy, Advanced Materials 29(23) (2017) 1606134.

[25] H. Zheng, Y. Zhang, L. Liu, W. Wan, P. Guo, A.M. Nyström, X. Zou, One-pot synthesis of metal-organic frameworks with encapsulated target molecules and their applications for controlled drug delivery, Journal of the American chemical society 138(3) (2016) 962-968.

[26] C. He, K. Lu, D. Liu, W. Lin, Nanoscale metal-organic frameworks for the co-delivery of cisplatin and pooled siRNAs to enhance therapeutic efficacy in drug-resistant ovarian cancer cells, Journal of the American Chemical Society 136(14) (2014) 5181-5184.

[27] A.R. Chowdhuri, D. Bhattacharya, S.K. Sahu, Magnetic nanoscale metal organic frameworks for potential targeted anticancer drug delivery, imaging and as an MRI contrast agent, Dalton Transactions 45(7) (2016) 2963-2973.

[28] J. Liu, Y. Yang, W. Zhu, X. Yi, Z. Dong, X. Xu, M. Chen, K. Yang, G. Lu, L. Jiang, Nanoscale metal- organic frameworks for combined photodynamic & radiation therapy in cancer treatment, Biomaterials 97 (2016) 1-9.

[29] K. Lu, C. He, W. Lin, A chlorin-based nanoscale metal-organic

framework for photodynamic therapy of colon cancers, Journal of the American Chemical Society 137(24) (2015) 7600-7603.

[30] W. Cai, H. Gao, C. Chu, X. Wang, J. Wang, P. Zhang, G. Lin, W. Li, G. Liu, X. Chen, Engineering Phototheranostic Nanoscale Metal-Organic Frameworks for Multimodal Imaging-Guided Cancer Therapy, ACS applied materials & interfaces 9(3) (2017) 2040-2051.

[31] M. Ma, H. Noei, B. Mienert, J. Niesel, E. Bill, M. Muhler, R.A. Fischer, Y. Wang, U. Schatzschneider, N. Metzler☐Nolte, Iron Metal-Organic Frameworks MIL☐88B and NH_2☐MIL☐88B for the Loading and Delivery of the Gasotransmitter Carbon Monoxide, Chemistry-A European Journal 19(21) (2013) 6785-6790.

[32] K.M. Taylor, W.J. Rieter, W. Lin, Manganese-based nanoscale metal- organic frameworks for magnetic resonance imaging, Journal of the American Chemical Society 130(44) (2008) 14358-14359.

[33] W.J. Rieter, K.M. Taylor, H. An, W. Lin, W. Lin, Nanoscale metal-organic frameworks as potential multimodal contrast enhancing agents, Journal of the American Chemical Society 128(28) (2006) 9024-9025.

[34] M. Vallet-Regi, A. Ramila, R. Del Real, J. Pérez-Pariente, A new property of MCM-41: drug delivery system, Chemistry of Materials 13(2) (2001) 308-311.

[35] H.J. Kim, H. Matsuda, H. Zhou, I. Honma, Ultrasound☐triggered smart drug release from a poly (dimethylsiloxane)-mesoporous silica composite, Advanced Materials 18(23) (2006) 3083-3088.

[36] B. Moulari, D. Pertuit, Y. Pellequer, A. Lamprecht, The targeting of surface modified silica nanoparticles to inflamed tissue in experimental colitis, Biomaterials 29(34) (2008) 4554-4560.

[37] J. Lu, M. Liong, Z. Li, J.I. Zink, F. Tamanoi, Biocompatibility, biodistribution, and drug☐delivery efficiency of mesoporous silica nanoparticles for cancer therapy in animals, Small 6(16) (2010) 1794-1805.

[38] A.E. Garcia-Bennett, Synthesis, toxicology and potential of ordered mesoporous materials in nanomedicine, Nanomedicine 6(5) (2011) 867-877.

[39] F. Tang, L. Li, D. Chen, Mesoporous silica nanoparticles: synthesis, biocompatibility and drug delivery, Advanced materials 24(12) (2012) 1504-1534.

[40] R. Mellaerts, J.A. Jammaer, M. Van Speybroeck, H. Chen, J.V. Humbeeck, P. Augustijns, G. Van den Mooter, J.A. Martens, Physical state of poorly water soluble therapeutic molecules loaded into SBA-15 ordered mesoporous silica carriers: a case study with itraconazole and ibuprofen, Langmuir 24(16) (2008) 8651-8659.

[41] D. Halamová, M. Badaničová, V. Zeleňák, T. Gondová, U. Vainio, Naproxen drug delivery using periodic mesoporous silica SBA-15, Applied Surface Science 256(22) (2010) 6489-6494.

[42] D. Halamová, V. Zeleňák, NSAID naproxen in mesoporous matrix MCM-41: drug uptake and release properties, Journal of inclusion

phenomena and macrocyclic chemistry 72(1-2) (2012) 15-23.

[43] D. Li, Y.-T. Zhang, M. Yu, J. Guo, D. Chaudhary, C.-C. Wang, Cancer therapy and fluorescence imaging using the active release of doxorubicin from MSPs/Ni-LDH folate targeting nanoparticles, Biomaterials 34(32) (2013) 7913-7922.

[44] A. Nieto, F. Balas, M. Colilla, M. Manzano, M. Vallet-Regí, Functionalization degree of SBA-15 as key factor to modulate sodium alendronate dosage, Microporous and Mesoporous Materials 116(1-3) (2008) 4-13.

[45] I. Izquierdo-Barba, E. Sousa, J.C. Doadrio, A.L. Doadrio, J.P. Pariente, A. Martínez, F. Babonneau, M. Vallet-Regí, Influence of mesoporous structure type on the controlled delivery of drugs: release of ibuprofen from MCM-48, SBA-15 and functionalized SBA-15, Journal of Sol-Gel Science and Technology 50(3) (2009) 421-429.

[46] M. Vallet Regí, F. Balas, D. Arcos, Mesoporous materials for drug delivery, Angewandte Chemie International Edition 46(40) (2007) 7548-7558.

[47] N.J. Halas, Nanoscience under glass: the versatile chemistry of silica nanostructures, ACS nano 2(2) (2008) 179-183.

[48] H. Deng, C.J. Doonan, H. Furukawa, R.B. Ferreira, J. Towne, C.B. Knobler, B. Wang, O.M. Yaghi, Multiple functional groups of varying ratios in metal-organic frameworks, Science 327(5967) (2010) 846-850.

[49] H.K. Chae, D.Y. Siberio-Perez, J. Kim, Y. Go, M. Eddaoudi, A.J. Matzger, M. O'keeffe, O.M. Yaghi, A route to high surface area, porosity and inclusion of large molecules in crystals, Nature 427(6974) (2004) 523.

[50] S.J. Garibay, Z. Wang, K.K. Tanabe, S.M. Cohen, Postsynthetic modification: a versatile approach toward multifunctional metal-organic frameworks, Inorganic chemistry 48(15) (2009) 7341-7349.

[51] Y. Li, L.-J. Wang, H.-L. Fan, J. Shangguan, H. Wang, J. Mi, Removal of sulfur compounds by a copper-based metal organic framework under ambient conditions, Energy & Fuels 29(1) (2014) 298-304.

[52] J.-R. Li, J. Sculley, H.-C. Zhou, Metal-organic frameworks for separations, Chemical reviews 112(2) (2011) 869-932.

[53] J.S. Seo, D. Whang, H. Lee, S. Im Jun, J. Oh, Y.J. Jeon, K. Kim, A homochiral metal-organic porous material for enantioselective separation and catalysis, Nature 404(6781) (2000) 982.

[54] L.J. Murray, M. Dincă, J.R. Long, Hydrogen storage in metal-organic frameworks, Chemical Society Reviews 38(5) (2009) 1294-1314.

[55] D. Cunha, M. Ben Yahia, S. Hall, S.R. Miller, H. Chevreau, E. Elkaïm, G. Maurin, P. Horcajada, C. Serre, Rationale of drug encapsulation and release from biocompatible porous metal-organic frameworks, Chemistry of Materials 25(14) (2013) 2767-2776.

[56] C. Le Bourlais, L. Acar, H. Zia, P.A. Sado, T. Needham, R. Leverge, Ophthalmic drug delivery systems—recent advances, Progress in retinal and eye research 17(1) (1998) 33-58.

[57] E.M. Del Amo, A. Urtti, Current and future ophthalmic drug delivery systems: a shift to the posterior segment, Drug discovery today 13(3-4) (2008) 135-143.

[58] K. Järvinen, T. Järvinen, A. Urtti, Ocular absorption following topical delivery, Advanced drug delivery reviews 16(1) (1995) 3-19.

[59] S. Kirchhof, A.M. Goepferich, F.P. Brandl, Hydrogels in ophthalmic applications, European Journal of Pharmaceutics and Biopharmaceutics 95 (2015) 227-238.

[60] Z.-x. He, Z.-h. Wang, H.-h. Zhang, X. Pan, W.-r. Su, D. Liang, C.-b. Wu, Doxycycline and hydroxypropyl-β-cyclodextrin complex in poloxamer thermal sensitive hydrogel for ophthalmic delivery, Acta Pharmaceutica Sinica B 1(4) (2011) 254-260.

[61] F. Gurtler, V. Kaltsatos, B. Boisramé, J. Deleforge, M. Gex-Fabry, L.P. Balant, R. Gurny, Ocular availability of gentamicin in small animals after topical administration of a conventional eye drop solution and a novel long acting bioadhesive ophthalmic drug insert, Pharmaceutical research 12(11) (1995) 1791-1795.

[62] M. Bhowmik, P. Kumari, G. Sarkar, M.K. Bain, B. Bhowmick, M.M.R. Mollick, D. Mondal, D. Maity, D. Rana, D. Bhattacharjee, Effect of xanthan gum and guar gum on in situ gelling ophthalmic drug delivery system based on poloxamer-407, International journal of biological macromolecules 62 (2013) 117-123.

[63] S. Bauer, C. Serre, T. Devic, P. Horcajada, J. Marrot, G. Ferey, N. Stock, High-throughput assisted rationalization of the formation of metal organic frameworks in the iron (III) aminoterephthalate solvothermal system, Inorganic chemistry 47(17) (2008) 7568-7576.

[64] A. Ahuja, R.K. Khar, J. Ali, Mucoadhesive drug delivery systems, Drug Development and industrial pharmacy 23(5) (1997) 489-515.

[65] D.A. Lee, E.J. Higginbotham, Glaucoma and its treatment: a review, American journal of health-system pharmacy 62(7) (2005) 691-699.

[66] J.Q. Dong, D.M. Babusis, D.F. Welty, A.A. Acheampong, D. Tang-Liu, S.M. Whitcup, Effects of the Preservative Purite® on the Bioavailability of Brimonidine in the Aqueous Humor of Rabbits, Journal of ocular pharmacology and therapeutics 20(4) (2004) 285-292.

[67] C. Yang, K. Chen, W. Hsu, Y. Li, Cytotoxicity of silicone oil on cultivated human corneal endothelium, Eye 22(2) (2008) 282.

[68] T. Tsai, W. Chen, F.-R. Hu, Comparison of fluoroquinolones: cytotoxicity on human corneal epithelial cells, Eye 24(5) (2010) 909.

[69] A.M. De Campos, Y. Diebold, E.L. Carvalho, A. Sánchez, M.J. Alonso, Chitosan nanoparticles as new ocular drug delivery systems: in vitro stability, in vivo fate, and cellular toxicity, Pharmaceutical research 21(5) (2004) 803-810.

[70] M. MANTLE, A. ALLEN, A colorimetric assay for glycoproteins

based on the periodic acid/Schiff stain, Portland Press Limited, 1978.

[71] P. He, S.S. Davis, L. Illum, In vitro evaluation of the mucoadhesive properties of chitosan microspheres, International journal of pharmaceutics 166(1) (1998) 75-88.

[72] C.G. Park, Y.K. Kim, M.J. Kim, M. Park, M.H. Kim, S.H. Lee, S.Y. Choi, W.S. Lee, Y.J. Chung, Y.E. Jung, Mucoadhesive microparticles with a nanostructured surface for enhanced bioavailability of glaucoma drug, Journal of Controlled Release 220 (2015) 180-188.

[73] C.G. Park, M.J. Kim, M. Park, S.Y. Choi, S.H. Lee, J.E. Lee, G.-S. Shin, K.H. Park, Y.B. Choy, Nanostructured mucoadhesive microparticles for enhanced preocular retention, Acta biomaterialia 10(1) (2014) 77-86.

[74] D.R. Korb, J.P. Herman, V.M. Finnemore, J.M. Exford, C.A. Blackie, An evaluation of the efficacy of fluorescein, rose bengal, lissamine green, and a new dye mixture for ocular surface staining, Eye & contact lens 34(1) (2008) 61-64.

[75] M.-H. Pham, G.-T. Vuong, A.-T. Vu, T.-O. Do, Novel route to size-controlled Fe–MIL–88B–NH_2 metal–organic framework nanocrystals, Langmuir 27(24) (2011) 15261-15267.

[76] S. Maiti, S. Paul, R. Mondol, S. Ray, B. Sa, Nanovesicular formulation of brimonidine tartrate for the management of glaucoma: in vitro and in vivo evaluation, AAPS PharmSciTech 12(2) (2011) 755-763.

[77] P. Horcajada, F. Salles, S. Wuttke, T. Devic, D. Heurtaux, G. Maurin, A. Vimont, M. Daturi, O. David, E. Magnier, How linker's modification controls swelling properties of highly flexible iron (III) dicarboxylates MIL-88, Journal of the American Chemical Society 133(44) (2011) 17839-17847.

[78] S. Mishima, A. Gasset, S. Klyce, J. Baum, Determination of tear volume and tear flow, Investigative Ophthalmology & Visual Science 5(3) (1966) 264-276.

[79] P. Bhagav, P. Deshpande, S. Pandey, S. Chandran, Development and validation of stability indicating UV spectrophotometric method for the estimation of brimonidine tartrate in pure form, formulations and preformulation studies, Der Pharmacia Lettre 2(3) (2010) 106-22.

[80] D.-W. Lee, S.A. Shirley, R.F. Lockey, S.S. Mohapatra, Thiolated chitosan nanoparticles enhance anti-inflammatory effects of intranasally delivered theophylline, Respiratory research 7(1) (2006) 112.

[81] D. Ghate, H.F. Edelhauser, Ocular drug delivery, Expert opinion on drug delivery 3(2) (2006) 275-287.

[82] A. Zimmer, J. Kreuter, Microspheres and nanoparticles used in ocular delivery systems, Advanced Drug Delivery Reviews 16(1) (1995) 61-73.

[83] T.R. Walters, Development and use of brimonidine in treating acute and chronic elevations of intraocular pressure: a review of safety, efficacy, dose response, and dosing studies, Survey of ophthalmology

41 (1996) S19–S26.

[84] D. Ball, J. Hill, R. Scott, The basics of general, organic, and biological chemistry, The Saylor Foundation2011.

[85] S.-N. Kim, J. Kim, H.-Y. Kim, H.-Y. Cho, W.-S. Ahn, Adsorption/catalytic properties of MIL-125 and NH_2-MIL-125, Catalysis today 204 (2013) 85–93.

[86] L. Alaerts, C.E. Kirschhock, M. Maes, M.A. Van Der Veen, V. Finsy, A. Depla, J.A. Martens, G.V. Baron, P.A. Jacobs, J.F. Denayer, Selective adsorption and separation of xylene isomers and ethylbenzene with the microporous vanadium (IV) terephthalate MIL□47, Angewandte Chemie International Edition 46(23) (2007) 4293–4297.

[87] N. Efremova, Y. Huang, N. Peppas, D. Leckband, Direct measurement of interactions between tethered poly (ethylene glycol) chains and adsorbed mucin layers, Langmuir 18(3) (2002) 836–845.

[88] I. Van-Seuningen, N. Houdret, A. Hayem, M. Davril, Strong ionic interactions between mucins and two basic proteins, mucus proteinase inhibitor and lysozyme, in human bronchial secretions, The International journal of biochemistry 24(2) (1992) 303–311.

[89] H. Zhu, A. Chauhan, A mathematical model for ocular tear and solute balance, Current eye research 30(10) (2005) 841–854.

[90] P. Jansook, E. Stefánsson, M. Thorsteinsdóttir, B.B. Sigurdsson, S.S. Kristjánsdóttir, J.F. Bas, H.H. Sigurdsson, T. Loftsson, Cyclodextrin solubilization of carbonic anhydrase inhibitor drugs: formulation of dorzolamide eye drop microparticle suspension, European journal of pharmaceutics and biopharmaceutics 76(2) (2010) 208–214.

[91] G. Tataru, M. Popa, D. Costin, J. Desbrieres, Microparticles based on natural and synthetic polymers for ophthalmic applications, Journal of Biomedical Materials Research Part A 100(5) (2012) 1209–1220.

[92] T. Peters, S.-W. Kim, V. Castro, K. Stingl, T. Strasser, S. Bolz, U. Schraermeyer, G. Mihov, M. Zong, V. Andres-Guerrero, Evaluation of polyesteramide (PEA) and polyester (PLGA) microspheres as intravitreal drug delivery systems in albino rats, Biomaterials 124 (2017) 157–168.

[93] Q. Pan, Q. Xu, N.J. Boylan, N.W. Lamb, D.G. Emmert, J.-C. Yang, L. Tang, T. Heflin, S. Alwadani, C.G. Eberhart, Corticosteroid-loaded biodegradable nanoparticles for prevention of corneal allograft rejection in rats, Journal of Controlled Release 201 (2015) 32–40.

[94] H.A. Salama, M. Ghorab, A.A. Mahmoud, M.A. Hady, PLGA Nanoparticles as subconjunctival injection for management of glaucoma, AAPS PharmSciTech 18(7) (2017) 2517–2528.

[95] Y. Diebold, M. Jarrín, V. Sáez, E.L. Carvalho, M. Orea, M. Calonge, B. Seijo, M.J. Alonso, Ocular drug delivery by liposome-chitosan nanoparticle complexes (LCS-NP), Biomaterials 28(8) (2007) 1553–1564.

[96] A.E. De Salamanca, Y. Diebold, M. Calonge, C. García-Vazquez, S.

Callejo, A. Vila, M.J. Alonso, Chitosan nanoparticles as a potential drug delivery system for the ocular surface: toxicity, uptake mechanism and in vivo tolerance, Investigative ophthalmology & visual science 47(4) (2006) 1416-1425.

[97] Ž. Vanić, N. Škalko-Basnet, Mucosal nanosystems for improved topical drug delivery: Vaginal route of administration, Journal of Drug Delivery Science and Technology 24(5) (2014) 435-444.

[98] M. Ma, A.l. Bétard, I. Weber, N.S. Al-Hokbany, R.A. Fischer, N. Metzler-Nolte, Iron-based metal–organic frameworks MIL-88B and NH$_2$-MIL-88B: high quality microwave synthesis and solvent-induced lattice "breathing", Crystal Growth & Design 13(6) (2013) 2286-2291.

[99] C. Marques Costa, L. Coli Louvisse de Abreu, E. Pereira dos Santos, O. Augusto Franca Presgrave, A.P. Trindade Rocha Pierucci, C. Rangel Rodrigues, V. Pereira de Sousa, S. Nicoli, E. Ricci Junior, L. Mendes Cabral, Preparation and evaluation of chitosan submicroparticles containing pilocarpine for glaucoma therapy, Current drug delivery 12(5) (2015) 491-503.

[100] T. Kean, M. Thanou, Biodegradation, biodistribution and toxicity of chitosan, Advanced drug delivery reviews 62(1) (2010) 3-11.

[101] I. Genta, B. Conti, P. Perugini, F. Pavanetto, A. Spadaro, G. Puglisi, Bioadhesive microspheres for ophthalmic administration of acyclovir, Journal of Pharmacy and Pharmacology 49(8) (1997) 737-742.

[102] X. He, P. Hahn, J. Iacovelli, R. Wong, C. King, R. Bhisitkul, M. Massaro-Giordano, J.L. Dunaief, Iron homeostasis and toxicity in retinal degeneration, Progress in retinal and eye research 26(6) (2007) 649-673.

[103] N.A. Peppas, J.R. Robinson, Bioadhesives for optimization of drug delivery, Taylor & Francis, 1995.

[104] L.H. Chuah, C.J. Roberts, N. Billa, S. Abdullah, R. Rosli, Cellular uptake and anticancer effects of mucoadhesive curcumin-containing chitosan nanoparticles, Colloids and Surfaces B: Biointerfaces 116 (2014) 228-236.

[105] N. Langoth, H. Kahlbacher, G. Schöffmann, I. Schmerold, M. Schuh, S. Franz, P. Kurka, A. Bernkop-Schnürch, Thiolated chitosans: design and in vivo evaluation of a mucoadhesive buccal peptide drug delivery system, Pharmaceutical research 23(3) (2006) 573-579.

[106] C. Menzel, S. Bonengel, I.P. de Sousa, F. Laffleur, F. Prüfert, A. Bernkop-Schnürch, Preactivated thiolated nanoparticles: A novel mucoadhesive dosage form, International journal of pharmaceutics 497(1-2) (2016) 123-128.

[107] C.-M. Lehr, Bioadhesion technologies for the delivery of peptide and protein drugs to the gastrointestinal tract, Critical reviews in therapeutic drug carrier systems 11(2) (1994) 119-160.

[108] D. Zhao, J. Feng, Q. Huo, N. Melosh, G.H. Fredrickson, B.F. Chmelka, G.D. Stucky, Triblock copolymer syntheses of mesoporous

silica with periodic 50 to 300 angstrom pores, science 279(5350) (1998) 548-552.

[109] C. Kresge, M. Leonowicz, W.J. Roth, J. Vartuli, J. Beck, Ordered mesoporous molecular sieves synthesized by a liquid-crystal template mechanism, nature 359(6397) (1992) 710.

[110] M.E. Davis, Ordered porous materials for emerging applications, Nature 417(6891) (2002) 813.

[111] I.I. Slowing, B.G. Trewyn, S. Giri, V.Y. Lin, Mesoporous silica nanoparticles for drug delivery and biosensing applications, Advanced Functional Materials 17(8) (2007) 1225-1236.

[112] M. Arruebo, M. Galán, N. Navascués, C. Téllez, C. Marquina, M.R. Ibarra, J. Santamaría, Development of magnetic nanostructured silica-based materials as potential vectors for drug-delivery applications, Chemistry of Materials 18(7) (2006) 1911-1919.

[113] J. Lu, M. Liong, J.I. Zink, F. Tamanoi, Mesoporous silica nanoparticles as a delivery system for hydrophobic anticancer drugs, small 3(8) (2007) 1341-1346.

[114] Z. Li, J.C. Barnes, A. Bosoy, J.F. Stoddart, J.I. Zink, Mesoporous silica nanoparticles in biomedical applications, Chemical Society Reviews 41(7) (2012) 2590-2605.

[115] A. Rahikkala, J.M. Rosenholm, H.A. Santos, Biofunctionalized Mesoporous Silica Nanomaterials for Targeted Drug Delivery, Biomedical Applications of Functionalized Nanomaterials, Elsevier2018, pp. 489-520.

[116] I.I. Slowing, J.L. Vivero-Escoto, C.-W. Wu, V.S.-Y. Lin, Mesoporous silica nanoparticles as controlled release drug delivery and gene transfection carriers, Advanced drug delivery reviews 60(11) (2008) 1278-1288.

[117] B.G. Trewyn, I.I. Slowing, S. Giri, H.-T. Chen, V.S.-Y. Lin, Synthesis and functionalization of a mesoporous silica nanoparticle based on the sol-gel process and applications in controlled release, Accounts of chemical research 40(9) (2007) 846-853.

[118] R. Gaudana, J. Jwala, S.H. Boddu, A.K. Mitra, Recent perspectives in ocular drug delivery, Pharmaceutical research 26(5) (2009) 1197.

[119] J. Smart, I. Kellaway, H. Worthington, An in vitro investigation of mucosa adhesive materials for use in controlled drug delivery, Journal of Pharmacy and Pharmacology 36(5) (1984) 295-299.

[120] M.J. Alonso, A. Sánchez, The potential of chitosan in ocular drug delivery, Journal of Pharmacy and Pharmacology 55(11) (2003) 1451-1463.

[121] T. Akingbehin, J.R. Villada, Metipranolol-associated granulomatous anterior uveitis, British journal of ophthalmology 75(9) (1991) 519-523.

[122] D.T. Chang, M.C. Herceg, R.A. Bilonick, L. Camejo, J.S. Schuman, R.J. Noecker, Intracameral dexamethasone reduces inflammation on the

first postoperative day after cataract surgery in eyes with and without glaucoma, Clinical ophthalmology (Auckland, NZ) 3 (2009) 345.

[123] A. Katiyar, S. Yadav, P.G. Smirniotis, N.G. Pinto, Synthesis of ordered large pore SBA-15 spherical particles for adsorption of biomolecules, Journal of Chromatography A 1122(1-2) (2006) 13-20.

[124] B.L. Newalkar, N.V. Choudary, P. Kumar, S. Komarneni, T.S. Bhat, Exploring the potential of mesoporous silica, SBA-15, as an adsorbent for light hydrocarbon separation, Chemistry of materials 14(1) (2002) 304-309.

[125] J.P. Hanrahan, A. Donovan, M.A. Morris, J.D. Holmes, Synthesis and swelling of large pore diameter mesoporous silica spheres, Journal of Materials Chemistry 17(37) (2007) 3881-3887.

[126] Y.B. Choy, J.-H. Park, M.R. Prausnitz, Mucoadhesive microparticles engineered for ophthalmic drug delivery, Journal of Physics and Chemistry of Solids 69(5-6) (2008) 1533-1536.

[127] N.A. Peppas, Y. Huang, Nanoscale technology of mucoadhesive interactions, Advanced drug delivery reviews 56(11) (2004) 1675-1687.

[128] I.A. Sogias, A.C. Williams, V.V. Khutoryanskiy, Why is chitosan mucoadhesive?, Biomacromolecules 9(7) (2008) 1837-1842.

[129] J.-H. Park, H. Jeong, J. Hong, M. Chang, M. Kim, R.S. Chuck, J.K. Lee, C.-Y. Park, The effect of silica nanoparticles on human corneal epithelial cells, Scientific reports 6 (2016) 37762.

[130] M. Kim, J.-H. Park, H. Jeong, J. Hong, W.S. Choi, B.-H. Lee, C.Y. Park, An Evaluation of the in vivo Safety of Nonporous Silica Nanoparticles: Ocular Topical Administration versus Oral Administration, Scientific Reports 7(1) (2017) 8238.

Abstract in Korean

국문 초록

이 논문은 안용 약물 전달 시스템에 있어 약물 치료 효과를 향상 시키기 위하여 개발된 초다공성 하이브리드 재료의 디자인, 합성, 표면 기능화, 분석 및 평가에 관한 것이다. 안용약물의 효과적인 안구내 전달을 위하여 나노약물전달 시스템이나 주사형 제형 및 삽입형 디바이스 등 다양한 방법이 시도되었으나 제제의 제작과정이 매우 복잡하여 상용화되기 어렵거나 투약 과정이 침습적인 이유로 환자의 순응도가 낮아 실제 임상에 적용하는 것에 어려움이 있었다. 이로 인해 실제 처방되는 안약물은 90% 이상 점안약물로 처방되며 따라서 점안약물의 약물전달효율을 높이기 위한 방안으로 점도를 높이거나 점막부착성 고분자를 혼입하여 약물의 체류시간을 길게 유지하려는 방법이 적용되어 왔다. 그러나 이러한 제형의 전안부 국소 투여는 눈의 깜박임 및 빠른 눈물 순환작용으로 인해 눈의 표면에서 점안제가 신속히 제거될 뿐만 아니라 대부분이 비루관을 통해 배액되기 때문에 낮은 약물 생체 이용률 (5 % 미만) 문제가 있다.

이를 해결하기 위하여, 눈에 국소 점안 약물 전달을 위한 새로운 운반체로서 금속 유기 골격체, $NH_2-MIL-88(Fe)$을 개발하였다. $NH_2-MIL-88(Fe)$는 점막부착성을 갖는 아민그룹을 포함하는 유기리간드와 Fe 이온을 이용하여 수열합성법을 통해 제조되었으며 분말 X 선 회절, 푸리에 변환 적외선 분석, 열 중량 분석, 전자 현미경 및 N_2 흡착−탈착 측정으로 구조를 확인하였다. 녹내장 치료약인 브리모니딘을 $NH_2-MIL-88(Fe)$에 담지 하였을 때, 약물이 121.3 μg/mg 탑재되었으며, 탑재된 약물은 입자의

세공을 통해서 서방출형상으로 최대 12 시간 동안 방출되었다. NH_2-MIL-88(Fe)/Br의 점막 접착 성은 in vitro 환경에서 뮤신 흡착 실험을 통해 평가 하였고, 토끼를 이용한 동물 실험에서 4 시간이상 전안부에 남아 있었다. 결과적으로, NH_2-MIL-88(Fe)/Br은 투여 후 토끼의 안방수에서 장기간에 걸쳐 브리모니딘 농도가 높게 나타났으며, 이는 약물 생체 이용률 및 활성 기간이 임상에서 사용하는 기존 제재인 알파간피 (Alphagan P) 보다 2 배 이상 증가한 결과였다. 따라서, NH_2-MIL-88(Fe)은 안구 약물의 향상된 생체 이용률을 제공하는 점안 약물 국소 전달을 위한 유망한 입자임을 확인하였다.

또한, 항염증 약물인 덱사메타손의 점안 국소 전달을 위한 아민기능화 SBA-15 입자 (즉, APS-SBA-15)을 개발하였다. 메조세공을 갖는 SBA-15 은 수열합성을 통해 제작하고 세공을 확보하기 위하여 소성하였으며, 이후 입자의 표면에 아민그룹을 그라프팅하였다. 표면에 도입된 아민으로 인해, 음이온 특성을 갖는 약물인 dexamethasone이 APS-SBA-15의 중형 기공에 68.23 µg/mg의 양으로 효과적으로 삽입되어 DXS@APS-SBA-15를 생성 할 수 있었고, 약물이 입자에서 24 시간 동안 지속적으로 방출되는 것을 확인하였다. In vitro 환경에서 뮤신과의 혼합실험에서 DXS@APS-SBA-15는 점막 접착 성을 나타내었으며, in vivo 실험에서 토끼 눈에 점안하여 관찰한 결과, DXS@APS-SBA-15는 안점막에 부착함으로써 눈 표면에 오래 거주하는 것을 확인하였다. 개발한 DXS@APS-SBA-15는 임상에서 기 사용하는 기존 제형인 Maxidex 제제에 비해 덱사메타손의 생체 이용률이 1.8 배 이상 향상된 결과를 보였다.

이 연구를 통해, 아민기능화 된 금속-유기 골격체, NH_2-MIL-88 (Fe) 및 아민기능화 다공성 실리카 입자, APS-SBA-15가 점막접착성 갖는 것을 확인하였다. 또한 개발한 입자에

생체이용도가 낮은 안용약물인 브리모니딘과 덱사메타손을 각각 탑재하였을때, 약물의 생체이용도가 약 2배가량 증가한 것을 확인하여 점안 약물 국소 투여 제제의 생체 이용률 향상을 위한 유망한 담체 임을 증명하였다. 본 결과를 토대로 아민기능화 초다공성입자의 안용 약물전달 시스템이 점안국소약물 투여에 효율적인 것을 확인하였으며, 이를 다양한 약물에 적용하여 기존에 잦은 점안이 필요했던 다수의 약물 제제에 있어 약물 투여의 불편함을 극복할 수 있을 것으로 생각한다. 또한 점막부착성 아민기능화 초 다공성 입자는 눈 뿐만 아니라 인체 내 여러 부위에 존재하는 점막을 이용하여 다양한 약물전달 시스템에 적용가능하기 때문에 본 연구를 기반으로 이를 이용한 획기적인 연구가 진행될 수 있기를 기대한다.